INFORMATION TO USERS

This manuscript has been reproduced from the microfilm master. UMI films the text directly from the original or copy submitted. Thus, some thesis and dissertation copies are in typewriter face, while others may be from any type of computer printer.

The quality of this reproduction is dependent upon the quality of the copy submitted. Broken or indistinct print, colored or poor quality illustrations and photographs, print bleedthrough, substandard margins, and improper alignment can adversely affect reproduction.

In the unlikely event that the author did not send UMI a complete manuscript and there are missing pages, these will be noted. Also, if unauthorized copyright material had to be removed, a note will indicate the deletion.

Oversize materials (e.g., maps, drawings, charts) are reproduced by sectioning the original, beginning at the upper left-hand corner and continuing from left to right in equal sections with small overlaps. Each original is also photographed in one exposure and is included in reduced form at the back of the book.

Photographs included in the original manuscript have been reproduced xerographically in this copy. Higher quality 6" x 9" black and white photographic prints are available for any photographs or illustrations appearing in this copy for an additional charge. Contact UMI directly to order.

UMI

A Bell & Howell Information Company
300 North Zeeb Road, Ann Arbor MI 48106-1346 USA
313/761-4700 800/521-0600

A MULTIDIMENSIONAL ANISOTROPIC STRENGTH CRITERION BASED ON KELVIN MODES.

By

YVES PIERRE ARRAMON

A dissertation submitted to the Graduate Faculty in Engineering, in partial fulfillment of the requirements for the degree of Doctor of Philosophy, the City University of New York

1997

This manuscript has been read and accepted by the Graduate Faculty in Engineering in satisfaction of the dissertation requirement for the degree of Doctor of Philosophy.

9/11/97
Date

Stephen C Cowin
Chair of Examining Committee

9/11/97
Date

Gerard J. Gruen
Executive Officer

STEPHEN COWIN
FERIDUN DELALE
SUSANNAH FRITTON
MORTEZA MEHRABADI
ALI SADEGH
Supervisory Committee

THE CITY UNIVERSITY OF NEW YORK

ABSTRACT

A MULTIDIMENSIONAL ANISOTROPIC STRENGTH CRITERION BASED ON KELVIN MODES.

By

Yves Pierre Arramon

Advisor: Professor Stephen Cowin

A new theory for the prediction of multiaxial strength of anisotropic elastic materials was proposed by Biegler and Mehrabadi (1993). This theory is based on the premiss that the total elastic strain energy of an anisotropic material subjected to multiaxial stress can be decomposed into dilatational and deviatoric modes. A multidimensional strength criterion may thus be formulated by postulating that the failure would occur when the energy stored in one of these modes has reached a critical value. However, the logic employed by these authors to formulate a failure criterion based on this theory could not be extended to multiaxial stress. In this thesis, an alternate criterion is presented which redresses the biaxial restriction by reformulating the surfaces of constant modal energy as surfaces of constant eigenstress magnitude. The resulting failure envelope, in a multidimensional stress space, is piecewise smooth. Each facet of the envelope is expected to represent the locus of failure data by a particular Kelvin mode. It is further shown that the Kelvin mode theory alone provides an incomplete description of the failure of some materials, but that this weakness can be addressed by the introduction of a set of complementary modes. A revised theory which combines both Kelvin and complementary modes is thus proposed and applied seven

example materials: an isotropic concrete, tetragonal paperboard, two orthotropic softwoods, two orthotropic hardwoods and an orthotropic cortical bone. The resulting failure envelopes for these examples were plotted and, with the exception of concrete, shown to produce intuitively correct failure predictions.

Some have moved on. Some have moved away. Some will stay on and some have even passed away. These kind souls have helped me reach this place in my life. Some have helped me out of love, friendship, selfless dedication or simply out of genuine kindness. It is unlikely that they even remember exactly how they helped. It will take me a lifetime to thank them. Let me begin today,

Thank you.

TABLE OF CONTENTS

1 **INTRODUCTION** 1

2 **FAILURE THEORIES FOR ISOTROPIC MATERIALS** 5

3 **FAILURE THEORIES FOR ANISOTROPIC MATERIALS** 10

3.1 **General Failure Theories** 13

3.2 **Modal Failure theories** 17

3.2.1 Modal Decomposition by Quadratic Stress Invariants Polynomials (Hashin, 1980) 18

3.2.2 Modal Decomposition by Strain Invariants (Feng, 1991) 23

3.2.3 Modal Decomposition by Projection operators (Kelvin modes) 24

4 **A REVISED MODAL FAILURE THEORY** 27

5 **APPLICATION OF MODAL FAILURE TO SELECTED MATERIALS** 39

5.1 **Determination of the Failure Envelope** 39

5.2 **Numerical Example: Concrete (Isotropic)** 42

5.3 **Numerical Example: Paperboard (Tetragonal) with biaxial data** . 47

Four Woods (Orthotropic) 52

5.4.1 Numerical example: (Softwood) Douglas Fir 53

5.4.2 Numerical Example: (Softwood) Sitka Spruce 59

5.4.3 Numerical example: (Hardwood) Yellow Birch 64

5.4.4 Numerical example: (Hardwood) Northern Red Oak 69

5.5 **Numerical example: Bovine Cortical Bone (Orthotropic)** 74

6 **DISCUSSION** 80

7 **CONCLUSIONS AND RECOMMENDATIONS** 85

7.1 **Recommendations and Future Outlook** 86

8 **APPENDIX** 88

9 **BIBLIOGRAPHY** 90

LIST OF TABLES

Table		Page
1	Symmetry conditions	- 11 -
2	Strengths and eigenstresses for Douglas Fir	- 55 -
3	Strengths and eigenstresses for Sitka Spruce	- 60 -
4	Strengths and eigenstresses for Yellow Birch	- 66 -
5	Strengths and eigenstresses for Northern Red Oak	- 70 -
6	Strengths and eigenstresses for Bovine Cortical Bone	- 76 -
7	Strengths and eigenstresses for Paperboard	- 89 -

LIST OF FIGURES

Figure		Page
1	Isotropic failure theories	- 6 -
2	Distortional and dilatational energy criteria	- 7 -
3	Synopsis of the anisotropic symmetries of linear elasticity	- 12 -
4	A partial synopsis of anisotropic yield criteria.	- 13 -
5	Tsai-Wu criterion for bovine cortical bone (Cowin, 1989).	- 16 -
6	Model of a transversely isotropic material (Hashin, 1980)	- 19 -
7	Failure criterion for T. I. (Hashin, 1980)	- 21 -
8	Two dimensional modal failure criterion for paperboard (Biegler *et al.*, 1993; Martin 1994)	- 27 -
9	Evaluation of the mode bounds	- 28 -
10	Plot of the three-dimensional mode bounds for paperboard	-31 -
11	Illustration of the modal failure's inability to account for different compressive and tensile strength (paperboard)	- 32 -
12	Illustration of the modal failure's inability to account for different compressive and tensile strength (concrete)	- 33 -
13	A modified modal failure criterion for concrete	- 34 -
14	A combined Kelvin and complementary modal failure theory for Paperboard (from uniaxial strength)	- 37 -
15	Modal failure envelope for concrete	- 46 -
16	Plot of empirical triaxial strength predictions for concrete	- 46 -

17 Modal failure envelope for paperboard (from biaxial strength) ..... - 51 -

18 Comparison of the paperboard biaxial strength predictions (Modal failure and Tsai-Wu) ..... - 52 -

19 Modal failure envelope for softwoods (douglas fir) ..... - 58 -

20 Modal failure envelope for softwoods (sitka spruce) ..... - 63 -

21 Modal failure envelope for hardwoods (yellow birch) ..... - 68 -

22 Modal failure envelope for hardwoods (northern red oak) ..... - 73 -

23 Modal failure envelope and Tsai-Wu for bovine cortical bone ..... - 79 -

1 INTRODUCTION

It is hard to imagine how design engineers could succeed in their endeavors without the ability to predict the failure of structural elements. It is therefore not surprising that failure theories for isotropic materials have been available for centuries and many have proven to be valuable tools. However, in the past several decades new man-made composite materials have become increasingly used in structural design. These generally anisotropic materials exhibit directionally dependant mechanical properties and thus the strength theories developed for isotropic materials are inapplicable for them. Out of necessity, several empirical criteria have been developed for the prediction of strength of these new materials. The principal motivation for these criteria has been the prediction of strength of laminates of composite materials. Thus almost all of these anisotropic criteria are only applicable to thin or thick shell configurations. However, increasingly complex designs will eventually require new strength criteria which are not limited to biaxial stress conditions. Biomechanical engineers have long been aware of the anisotropic nature of the mechanical properties of organic materials. Wood and bone are materials which exhibit such a directionally dependent strength and stiffness. The stress states that these materials may be subjected to are generally multiaxial, more complex and therefore beyond the applicable range of biaxial strength criteria. Unfortunately, multidimensional strength criteria have not been forthcoming. Some of the currently available criteria are theoretically extendable to stress states other than biaxial, but present both difficulties in their implementation and limitations in their results when such an extension is attempted. With few exceptions these criteria are simply various implementations of empirical correlation curves. The complete

determination of these correlations becomes unusually difficult and impractical when applied to multiaxial stress. Furthermore, because these criteria are empirical, their strength predictions are at best only interpolative. With one exception, none of these multiaxial anisotropic strength criteria can be considered genuine theories. The object of this thesis is to investigate a recent candidate for a multiaxial anisotropic failure theory and to suggest that this candidate is a genuine theory and a viable alternative to the current crop of failure criteria.

The principles for the development of eigentensors of linear anisotropic elasticity were first introduced in 1856 by Lord Kelvin and rediscovered Rychlewski (1984) and by Mehrabadi and Cowin (1990). Extending the concepts associated with isotropic elastic materials, namely that stress and strain may be decomposed into its dilatational and deviatoric parts, Mehrabadi and Cowin state the following general properties for anisotropic eigentensors:

A. *For any elastic symmetry the total stress tensor and the total strain tensor can be additively decomposed into a sum of six or fewer eigentensors of identical form.*

B. *For any elastic symmetry each eigenstress is directly proportional to associated eigenstrain.*

C. *For any elastic symmetry there is an additive decomposition of the total strain energy into a sum of six or fewer terms, each term being a scalar-valued product of the stress and strain eigentensors of identical form. These terms represent energy modes which are not interactive.*

Property C allowed Biegler and Mehrabadi (1993) to suggest an extension of the von Mises plasticity theory to anisotropic materials. Their study shows how a strength criterion may be developed for anisotropic elastic materials by postulating that failure would occur when any of the dilatational or deviatoric parts of the strain energy would exceed a critical value. Unlike the Tsai-Wu and its variants which restricts the shape of the failure envelope to that of an ellipsoid, this criterion would exhibit modes of failure or Kelvin modes. The failure envelope, in this case, would be piecewise smooth in a multidimensional stress space. Thus polyhedral envelopes of various shapes and aspect ratios are possible. Each facet of the envelope would represent the locus of failure data by a specific Kelvin mode. The premiss this theory is based on is that failure occurs when the energy in any of the Kelvin modes has reached a critical value. The failure envelope which results from this premiss is therefore an explicit predictor of strength whereas an empirical correlation such as the Tsai-Wu can only offer an implicit one.

This theory and its application will be the basis for this thesis. In the following sections a short review of isotropic failure theories, with particular emphasis on von Mises plasticity, will be presented. A review of anisotropic failure criteria will follow. Emphasis will be placed on the Tsai-Wu criterion (Tsai and Wu, 1970) and on those criteria which attempt to predict modes of failure. The failure theory of Biegler and Mehrabadi (1993) will be introduced. A modified procedure for the determination of the failure bounds will be proposed. This revised procedure will accommodate the extension of the two-dimensional analysis of Biegler and Mehrabadi (1993) to a complete multidimensional theory. It will be further shown that this Kelvin mode theory provides an incomplete description of the failure

of some materials, but that this weakness can be addressed by the introduction of a set of complementary modes. This combined modal theory will be applied to several examples of materials. The resulting failure envelopes for these examples will be plotted in principal stress space and the implication of their strength predictions discussed. For those examples for which a Tsai-Wu criterion is available, the predictions of both criteria will be compared.

2 FAILURE THEORIES FOR ISOTROPIC MATERIALS

A brief review of several of the commonly accepted failures criteria for isotropic materials provides a basis of comparison with the anisotropic theories and serves to introduces those anisotropic theories which have been extended from the isotropic ones. For the purpose of this study, these theories are loosely grouped into two categories: those which assume that the compressive and tensile strength must be equal [Fig. 1(a)] and those which do not [Fig. 1(b)].

Maximum shear stress or *Tresca's* theory (sometimes called *Guest's Theory*) falls into the first category. The failure is assumed to occur at a point when the maximum shear stress has reached a critical value. It has been used with good results on ductile materials.

Though the *maximum strain energy* is sometimes mentioned in the literature it has been largely superseded by the more accurate *maximum distortional energy* theory (Huber, 1904; von Mises, 1913; and Henky, 1925). This theory uses the fact that the total strain energy exerted on an isotropic material is the sum of the *distortional* and *dilatational* energies. The theory postulates that the energy associated with the distortion of a material under biaxial stress determines the onset of yielding, or, in terms of the principal stresses, that,

$$(\sigma_1 - \sigma_2)^2 + (\sigma_2 - \sigma_3)^2 + (\sigma_3 - \sigma_1)^2 = 2\sigma_{yp}^2, \qquad (1)$$

where σ_{yp} is the uniaxial tensile yield stress.

This failure envelope in a principal stress space is an infinite tube with its axis oriented along the median vector [Fig. 2 (b)]. The fact that this failure tube is open ended is often ignored since the hydrostatic yield for many materials is quite high (Bridgeman, 1923;

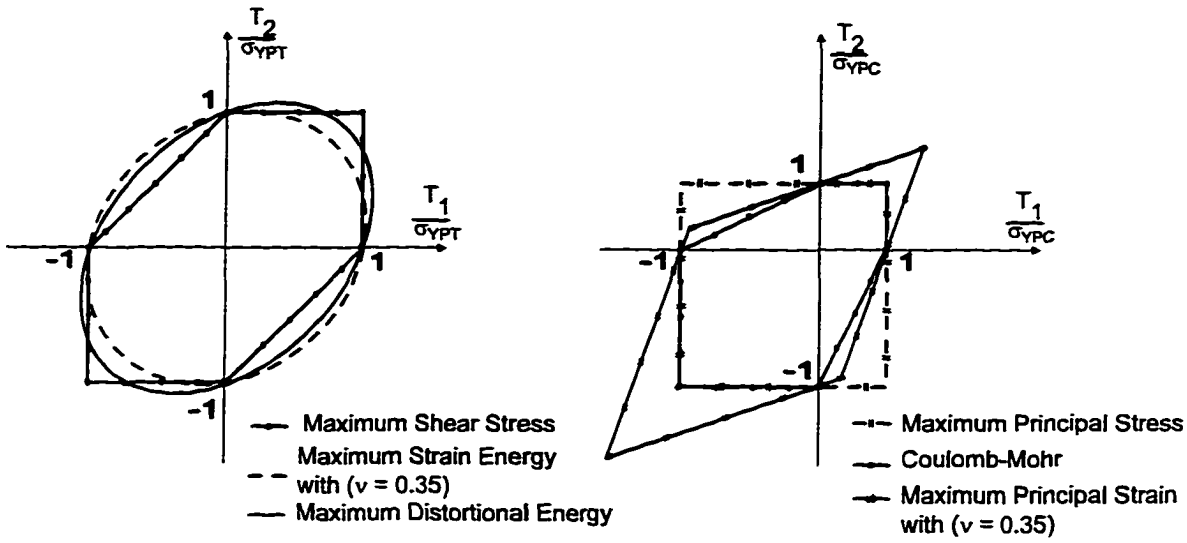

(a) (b)

Fig. 1 Illustration of the isotropic failure theories which assume the tensile and compressive strength: (a) are equal, (b) are different. The biaxial failure envelopes plots are normalized to the compressive yield point σ_{YPC} for (a) and the compressive yield point σ_{YPC} for (b).

Nadai, 1950). A complete three-dimensional failure theory for isotropic materials would include two yield criteria, one for a distortional mode of failure (maximum von Mises) and one for a dilatational mode such as a maximum hydrostatic stress. The dilatational mode failure surface would be that of a plane normal to the axis of the von Mises tube and capping each end of it. As a consequence of this theory a complementary dilatational criterion is applied for triaxial stress, that is,

$$\frac{1}{3}(\sigma_1 + \sigma_2 + \sigma_3) = \sigma_H, \qquad (2)$$

where σ_H is the hydrostatic failure stress.

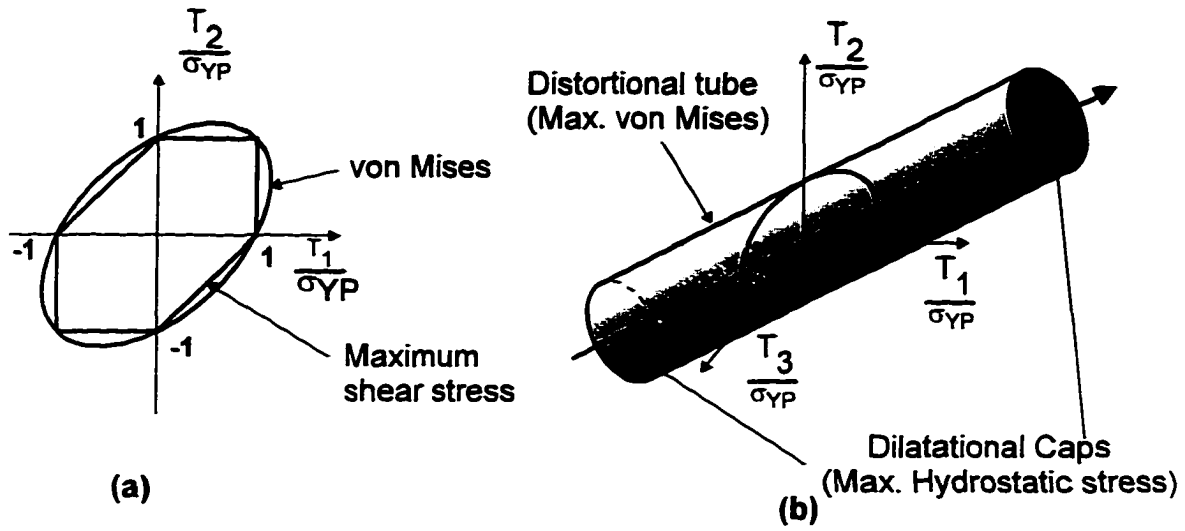

Fig. 2 Illustration of the three-dimensional distortional energy envelope along with the dilatational ends (b). The Maximum shear stress is sometimes used as an alternative to the von Mises criterion (a).

The *maximum octahedral* or *von Mises* criterion predicts the onset of yielding occurs when the shear stress acting on an octahedral plane of a point has reached a prescribed limit. It can be demonstrated that this criterion produces the same failure envelope as the maximum distortional strain energy criterion and is related to the latter by

$$U_{distortional} = \frac{3}{2}\frac{1+\nu}{E}\tau_{oct}^2 . \qquad (3)$$

This theory (along with maximum distortional energy) is widely accepted as most suitable in predicting the failure of isotropic ductile materials under multiaxial stress.

The formulations of these theories do not allow for distinct compression and tensile failure strengths and therefore are unsuitable for material with this characteristic. Other theories have been proposed which can accommodate this difference [Fig. 1(b)].

The *maximum principal stress* theory, sometimes called *Rankine's theory,* predicts

that a material will fail when the largest and smallest of the three principal stresses exceed either the material's prescribed tensile or compressive limit respectively. Though biaxial tests of ductile materials have failed to confirm the correctness of this theory it is still successfully applied to brittle materials.

Coulomb's Theory is sometimes called *Coulomb-Mohr's* theory because, like *Mohr's* theory, it predicts that failure will occur when the shear stress has reached some maximum value. But whereas Tresca assumed that the maximum shear criterion is a constant, Mohr's suggested that the shear was related to the principal stress by an experimentally determined function. That is,

$$|\tau| = F(\sigma). \tag{4}$$

Coulomb's theory extends this idea by suggesting that this function is

$$|\tau| = c - \mu \sigma, \tag{5}$$

where c is a measure of the cohesive strength of the material, μ is the frictional coefficient of failure plane inclined at ($\pi/4$ - ½ arctan μ) and σ is the normal stress acting on that plane. Although for metals and crystalline materials Tresca's or von Mises theories are usually favored, Coulomb's produces acceptable prediction for soils.

Maximum principal strain or *St. Venant's theory* predicts that failure will occur when the maximum principal strain exceeds the uniaxial yield strain. Although this theory is not nearly as popular as those described above, it is mentioned here because it has been successfully extended to the failure of laminates.

The popularity of some of these theories is often less dependent upon their accuracy than on their conservative predictions. For instance, although Coulomb's theory is often used

to predict the strengths of aggregates (concrete, soils, sands, etc.), experimental testing suggests that it may underestimate the strengths in biaxial stress states (concrete: Kupfer, 1973; sands: Green and Bishop, 1969; clays: Lade and Musante, 1978). For those materials that do not fit the general case, empirical curves have been formulated to accommodate their particularities (Podgórski, 1983).

3 FAILURE THEORIES FOR ANISOTROPIC MATERIALS

The failure theories described in the previous section are restricted to elastically isotropic materials. However, composites such as laminates, fibrous materials such as textiles and woods and biological materials such as bone, ligaments/tendons and skin all share the characteristic that their strength and stiffness are directionally dependent. These generally anisotropic materials display more complex interaction of multiaxial stresses and strains, making the development of reliable failure theories more difficult. Fortunately, it is possible to categorize many materials of similar elastic behavior into groups. Cowin and Mehrabadi (1995b) provide such a categorization. Their concept of "plane of mirror" or "reflective symmetry" provides a description of groups of anisotropic symmetries of which isotropy is one. The restrictions on the elastic constants are a consequence of this formulation and are summarized in table 1.

A synopsis of the symmetries catalogued by Cowin and Mehrabadi (1995b) with a correction (Cowin, Private Communication, 1996) is presented in Fig. 3. These symmetries are categorized by the number of planes of material symmetry and the arrows indicate the transition from one possible symmetry to another. For example, the addition of a second plane of symmetry, at an angle of $\pi/4$ to the single plane symmetry of a monoclinic material, naturally generates all the symmetry planes of a tetragonal material. The remainder of this study will refer to these symmetries (Fig. 3) and their restrictions (table 1) when describing a specific anisotropy.

Table 1 List of distinct symmetries and their properties derived from Cowin and Mehrabadi (1995b). Note that some corrections have been made to the restrictions and an additional "Pentagonal" symmetry is identified (Cowin, Priv. Com., 1996).

Material Symmetry	Number of Planes of Symmetry	Number of planes of Isotropy	Number of Independent Elastic Coef..	Restrictions on the Elastic Coefficients
Triclinic	0	0	21	None
Monoclinic	1	0	12	$c_{} =c_{} =c_{} =c_{} =c_{} =c_{} =c_{} =c_{} =0$ and $c_{} =0$ or $c_{} =0$
Orthotropic or Orthorombic	3	0	9	All the conditions for monoclinic plus $c_{41}=c_{42}=c_{43}=c_{56}=0$.
Tetragonal	5	0	6	All the conditions of orthotropic plus $c_{11}=c_{22}$, $c_{23}=c_{13}$, $c_{55}=c_{44}$,
Trigonal	3	0	6	$c_{} =c_{} =c_{} =c_{} =c_{} =c_{} =c_{} =0$, $c_{11}=c_{22}$, $c_{13}=c_{23}$, $c_{44}=c_{55}$, $-c_{42}=c_{56}=c_{14}$, $-c_{15}=c_{25}=c_{46}=0$ and $c_{66}=c_{11}-c_{22}$
Hexagonal	7	0	5	All the conditions of trigonal plus $-c_{42}=c_{56}=c_{14}=0$.
Pentagonal	5	0	5	Same as for Hexagonal
Transverse Isotropy	∞^1+1	1	5	Same as for Hexagonal
Cubic	9	0	3	All the conditions of Tetragonal plus $c_{11}=c_{33}$, $c_{12}=c_{13}$, $c_{44}=c_{66}$,
Isotropy	∞ 2	∞^2	2	or all the conditions for Cubic plus $c_{44}=(c_{11}-c_{12})/2$.

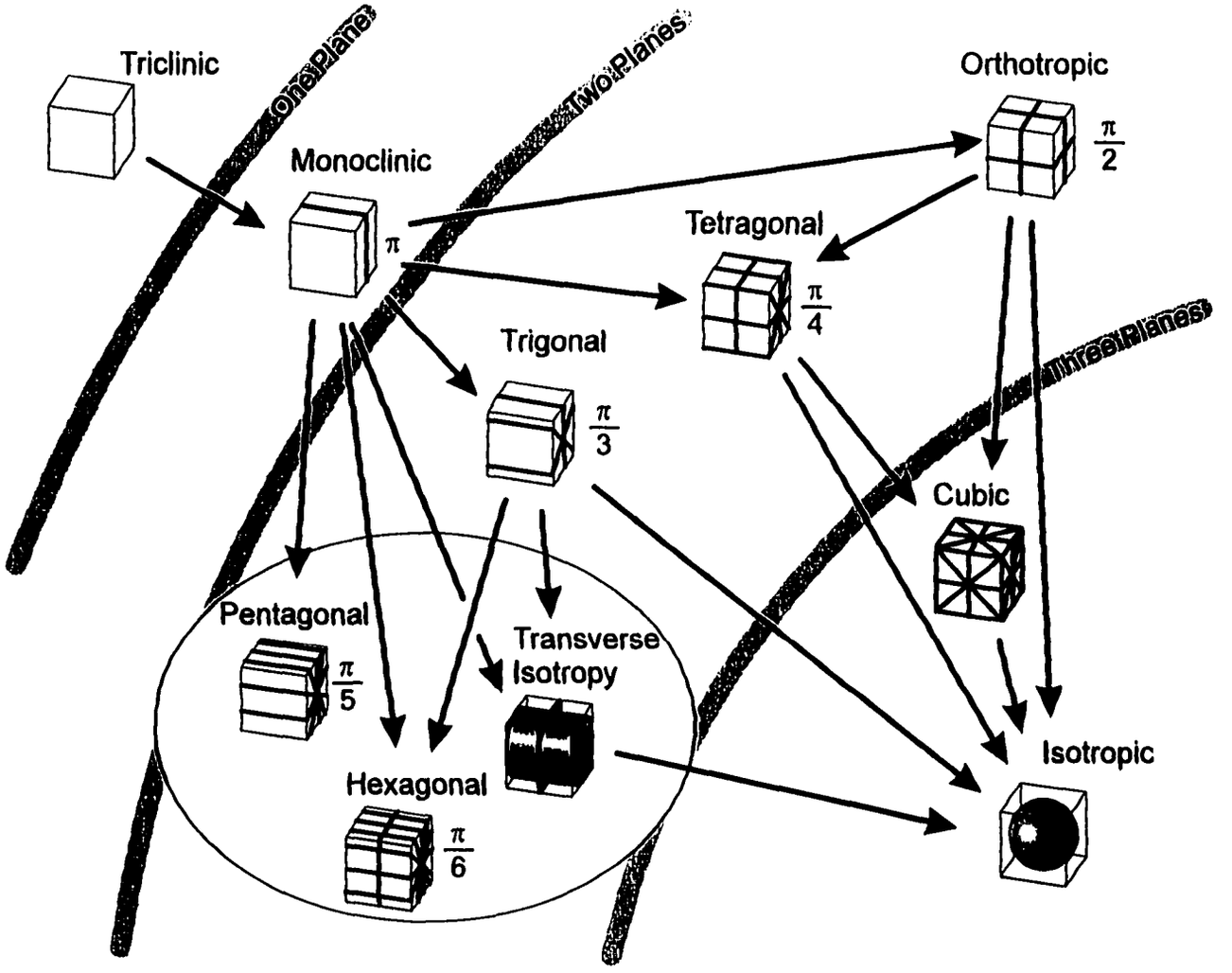

Fig. 3 A synopsis of the anisotropic symmetries of linear elasticity catalogued by Cowin and Mehrabadi (1995b) with the corrections (Cowin Priv. Com. 1996). Each arrow indicates the transition from one symmetry to another by the introduction of an additional plane of symmetry. For example, the addition of a plane of symmetry at $\pi/2$ to a monoclinic symmetry produces an orthotropic symmetry.

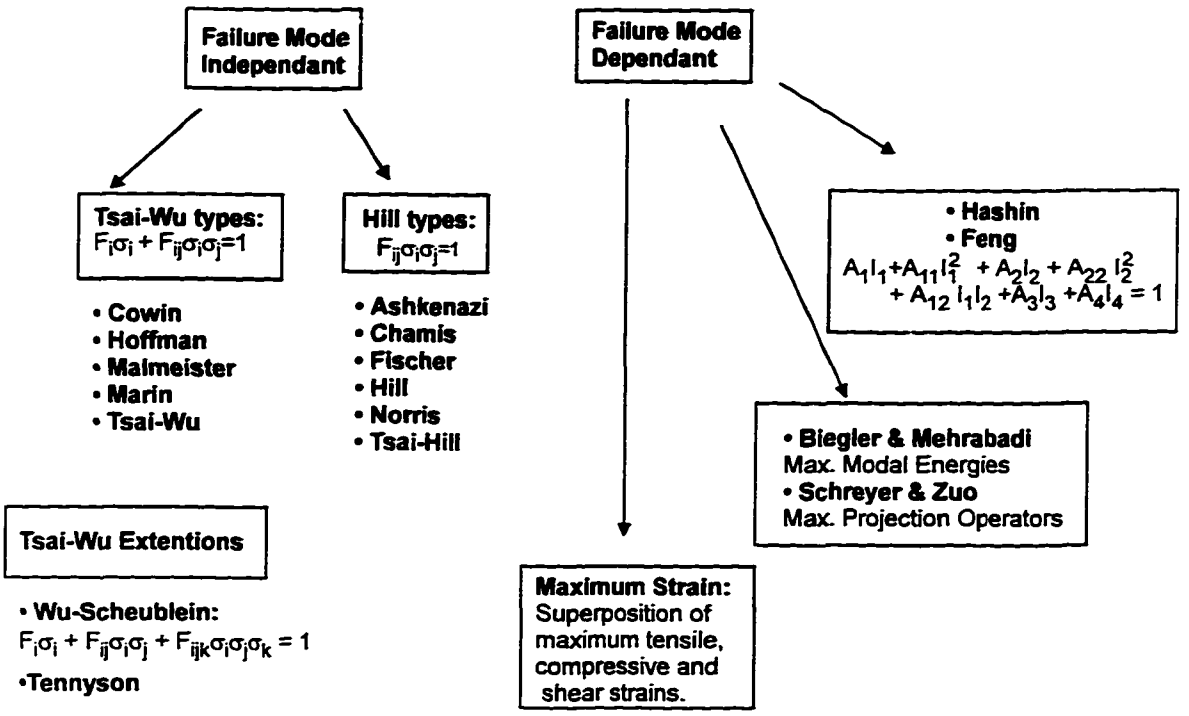

Fig. 4 A partial synopsis of anisotropic yield criteria. The left column lists those yield criteria which make no allowances for the "mode" of failure. The failure envelope is always one smooth surface. The right column lists those theories which may account for modes of failure. The envelopes for these theories are piecewise smooth.

3.1 General Failure Theories

A thorough review of the anisotropic strength theories which have been proposed up to 1985 is provided in Rowlands (1985). There are several theories that have been used with success. These usually assume that the failure envelope in a stress or strain space is a single function. The *Tsai-Hill* theory, for instance, assumes the multiaxial failure is bound by a closed quadratic surface, an ellipsoid. The failure bound in terms of the principal stresses T_i is described by

$$F_{ij}T_iT_j = 1, \tag{6}$$

where $I, j = 1,..., 6$ and F_{ij} are coefficients determined from mechanical tests (Hill, 1950). The *Tsai-Wu* failure criterion is a quadratic surface of the form

$$F_{ij}T_iT_j + F_iT_i = 1, \tag{7}$$

where $I, j = 1,..., 6$, F_i and F_{ij} are the second and fourth rank strength tensors, the coefficients of which are determined from mechanical tests (Tsai and Wu, 1970). In this theory however, the surface definition provides for the possibility of different compressive and tensile strengths. Most of the other theories suggested so far are variations of these two basic forms. Some like Cowin (1979) and Hoffman (1967) provide predictions of the F_{ij} and F_i coefficients. Others like Tennyson (1980) and Wu (1974) extend the Tsai-Wu criterion to include additional cubic terms (Fig. 4).

Although the Tsai-Wu failure criterion and its variants have found considerable acceptance in the literature, it appears that this is mainly based on its agreement with the two-dimensional experimental data. Close examination of the tensor polynomial (7) and the constraints on the stress interaction terms F_{ij} (Tsai and Wu, 1970),

$$F_{ii}F_{jj} - F_{ij}^2 \geq 0, \tag{8}$$

suggests that it is more apt at fitting the biaxial stress failure data than it is in providing a full three-dimensional failure envelope. For example, the quadratic surface illustrated in Fig. 5 is the three-dimensional Tsai-Wu strength criterion for bovine cortical bone provided by Cowin (1989) as

$$\begin{aligned} 20.38T_{11} + 13.33T_{22} + 2.2T_{33} + 135T_{11}^2 + 133.3T_{22}^2 + 27T_{33}^2 + 322T_{12}^2 + 229.3T_{13}^2 + 200.5T_{23}^2 \\ -2(26.9)T_{11}T_{22} - 2(54.4)T_{11}T_{33} - 2(39.2)T_{22}T_{33} = 1, \end{aligned} \tag{9}$$

where the units of the stress matrix components are GPa. This strength criterion is in good agreement with the available biaxial strength of cortical bone and has been well accepted. But even though this surface fits the biaxial failure data on all stress planes and satisfies restriction (8), it is not an ellipsoid. In fact this Tsai-Wu condition has no bound in triaxial compression and therefore would be unsuitable to describe any three-dimensional strength. The reason for this result is that the constraints on the stress interaction terms F_{ij} suggested in (Tsai and Wu, 1970) are necessary, but insufficient to guarantee that the strength tensor F be positive definite. Therefore, in a principal stress space, the Tsai-Wu criterion (7) with the restriction (8) is not a true three-dimensional criterion, but in fact, a set of three two-dimensional criteria. Each the two-dimensional Tsai-Wu ellipse is independently fitted to biaxial data by adjusting the appropriate stress interaction terms F_{12}, F_{13} or F_{23}. In order to guaranty that the strength data is fitted to an ellipsoid, the investigator would be required to simultaneously adjust all three stress interaction terms while verifying that the strength tensor is positive definite for each adjustment. This would be a very difficult task to accomplish and even if successful, it is unlikely that the resulting failure surface could fit the biaxial data as well as (7) with (8).

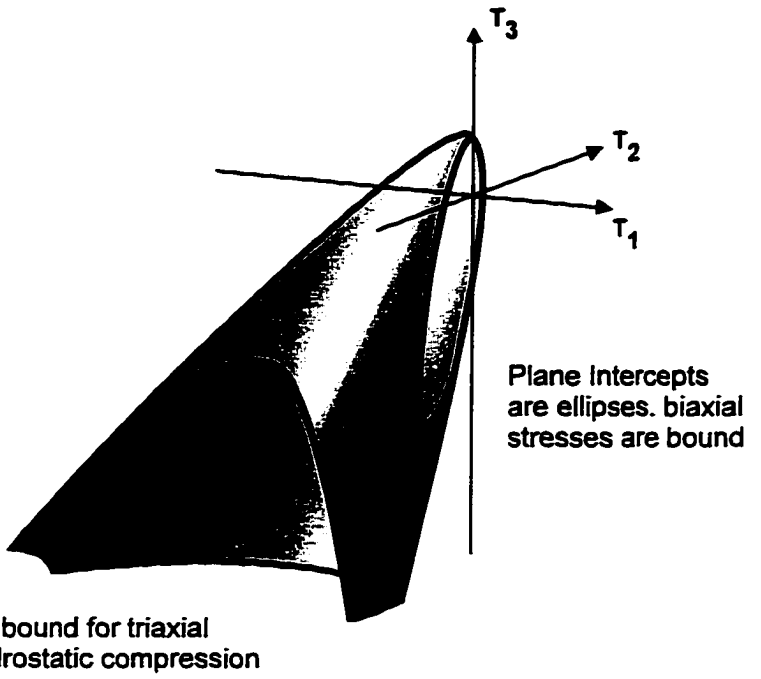

Fig. 5 Example of a limitation for a Tsai-Wu failure criterion. This surface is a three-dimensional representation of the Tsai-Wu criterion (9) for bovine cortical bone provided by Cowin (1989). This plot, in principal stress space, is unbounded for triaxial hydrostatic stress. Even though the criterion satisfies the restriction specified by Tsai and Wu (1970), it provides an incomplete description of the three-dimensional failure envelope.

In 1974, Wu and Scheublein suggested that the principal directions of strength need not be orthogonal and hence the failure surface is not necessarily an ellipsoid (Wu and Scheublein, 1974). They thus suggest that third-order terms be included in the tensor polynomial (7) so that the failure envelope becomes

$$F_i T_i + F_{ij} T_i T_j + F_{ijk} T_i T_j T_k = 1 . \qquad (10)$$

This extension to the theory allows the possibility that biaxial intercepts are the same ellipse as in the quadratic form of the Tsai-Wu criterion (7) and still describe a closed failure envelope. However, the determination of the constants of (10) would require several triaxial and combined tensile and shear tests. These tests are extremely difficult to accomplish accurately and therefore limit the usefulness of such a theory.

When used to predict the strength of planar components such as laminates, the Tsai-Wu often produces good results. However, tempting as it may be to extend the Tsai-Wu to three dimensions, this is not easily accomplished. Furthermore, theories such as Tsai-Wu assume that the three-dimensional failure envelope can be described by a single function. In practice, however, many materials exhibit multiple failure mechanisms so that the failure data may not be smoothly distributed. An appropriate single function would be either too complex to be determined or too simple to accurately describe the failure data distribution. This has led some investigators to believe that an appropriate failure envelope for anisotropic materials should not be produced from a single function, but rather from a set of functions. Each of these functions would describe the failure of a material by a particular mode of failure.

3.2 **Modal Failure theories**

In an attempt to correlate a failure mechanism, or a failure mode, with the failure envelope, some investigators have introduced modal failure theories (Hashin, 1980; Biegler and Mehrabadi, 1993). The premise of such theories is that anisotropic materials may fail by multiple independent mechanisms; therefore, their failure bounds in a stress or strain space are not required to be smooth, but simply piecewise smooth (Hashin, 1980). The failure envelopes for such materials would therefore be a composite of patches. Each patch represents the locus of failure by a particular mode. For instance the *Maximum Strain* theory predicts that failure will occur in a unidirectionally reinforced composite when either the maximum axial, transverse or shear strain is exceeded. The failure envelope of a laminate

composed of multiple layers of uniaxial plies may be produced by superimposing the individual ply predictions. Practical application of such a theory, however, is limited to biaxial stress or strain. Modal theories such as those suggested by Hashin (1980) and Feng (1991) provide a complete three-dimensional failure envelope for transversely isotropic materials. The criteria for these modes of failure are selected because their formulation only involves macroscopic stresses significant to a specific microscopic interaction. Other three-dimensional failure envelopes such as those produced by Biegler and Mehrabadi (1993) and Schreyer and Zuo (1995) are based on the premise that the symmetry of the failure envelope is related to that of the elasticity tensor. Unlike the maximum strain theory, these modal criteria have not been correlated with experimentally observed failure mechanisms. Therefore the relationship between failure mode and failure mechanism is, so far, mostly based on intuition.

3.2.1 Modal Decomposition by Quadratic Stress Invariants Polynomials (Hashin, 1980)

A modal failure criterion for transversely isotropic composite materials based upon the stress invariants was introduced by Hashin (1980). This criterion is assumed to be a function of the stress invariants I_k (where k=1..5 for transverse isotropy)

$$\begin{aligned} I_1 &= \sigma_{11}, \\ I_2 &= \sigma_{22} + \sigma_{33}, \\ I_3 &= \sigma_{23}^2 - \sigma_{22}\sigma_{33} \quad \text{or} \quad \frac{1}{4}(\sigma_{22} - \sigma_{33})^2 + \sigma_{23}^2, \\ I_4 &= \sigma_{12}^2 + \sigma_{13}^2, \\ I_5 &= 2\sigma_{12}\sigma_{23}\sigma_{13} - \sigma_{22}\sigma_{13}^2 - \sigma_{33}\sigma_{12}^2. \end{aligned} \tag{11}$$

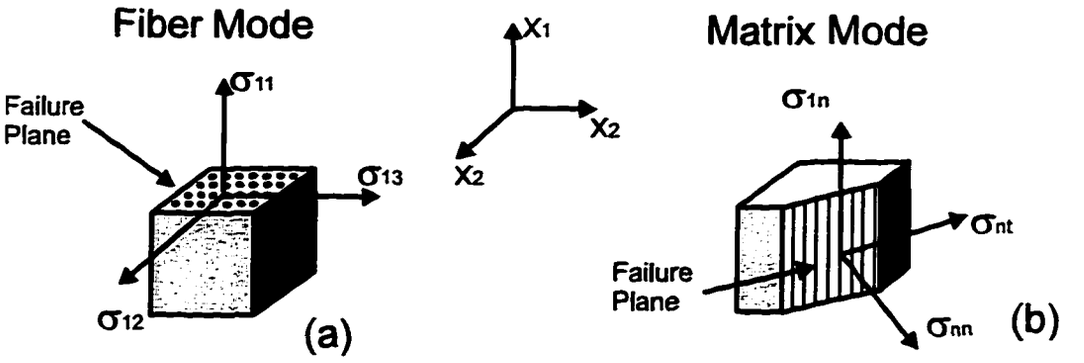

Fig. 6 Illustration of the failure modes for a transversely isotropic material. Hashin (1980) used this concept to describe how some of the stress may be exclusively associated with a failure of the fibers (a) and others with a failure of the matrix (b).

The criterion proposed by Hashin is the following quadratic approximation

$$A_1 I_1 + A_{11} I_1^2 + A_2 I_2 + A_{22} I_2^2 + A_{12} I_1 I_2 + A_3 I_3 + A_4 I_4 = 1, \tag{12}$$

which, in terms of the stresses, is given by

$$\begin{aligned} A_1\sigma_{11} + A_{11}\sigma_{11}^2 + A_2(\sigma_{22} + \sigma_{33}) + A_{22}(\sigma_{22} + \sigma_{33})^2 \\ + A_{12}\sigma_{11}(\sigma_{22} + \sigma_{33}) + A_3(\sigma_{23}^2 - \sigma_{22}\sigma_{33}) + A_4(\sigma_{12}^2 + \sigma_{13}^2) = 1. \end{aligned} \tag{13}$$

Hashin observes that some stresses are pertinent to failure in a fiber failure plane and others in a matrix failure plane (Fig. 6). By segregating these stress terms, the failure criterion (13) can be decoupled into two modal criteria:

a fiber mode:

$$A_1\sigma_{11} + A_{11}\sigma_{11}^2 + A_4(\sigma_{12}^2 + \sigma_{13}^2) = 1 \tag{14}$$

and a matrix mode:

$$A_2(\sigma_{22} + \sigma_{33}) + A_{22}(\sigma_{22} + \sigma_{33})^2 + A_3(\sigma_{23}^2 - \sigma_{22}\sigma_{33}) + A_4(\sigma_{12}^2 + \sigma_{13}^2) = 1. \quad (15)$$

It should be noted that the principal stress interaction term A_{12} in (13) is ignored. Hashin argues that this interaction may be negligible. Hashin further argues that since the failure mechanisms are different for tension and compression, the fiber and matrix modes must be solved for compression and tension separately. This produces a total of four surfaces, the constants of which must be determined from experiment. However, it becomes apparent from examining (14) that the determination of these constants would require several combined torsion/tensile tests. Hashin approximates this last information by requiring that the plot of the axial tensile/shear failure envelope is an ellipse with intercept σ_A and τ_A. Thus (14) may be rewritten as a set of two criteria: a tensile and a compressive fiber mode. Hashin gives the tensile fiber mode as,

$$\left(\frac{\sigma_{11}}{\sigma_A^+}\right)^2 + \frac{1}{\tau_A^2}(\sigma_{12}^2 + \sigma_{13}^2) = 1, \quad (16)$$

where σ_A^+ is the axial tensile strength and τ_A the axial shear strengths.

The compressive fiber mode reduces to

$$\sigma_{11} = \sigma_A^-, \quad (17)$$

where σ_A^- is the axial compressive failure data and the shear dependence is assumed to be negligible.

A similar reasoning was applied to the matrix modes so that (15) is rewritten as a tensile matrix mode

$$\frac{1}{(\sigma_T^-)^2}(\sigma_{22} + \sigma_{33})^2 + \frac{1}{\tau_T^2}(\sigma_{23}^2 - \sigma_{22}\sigma_{33}) + \frac{1}{\tau_A^2}(\sigma_{12}^2 + \sigma_{13}^2) = 1, \tag{18}$$

where σ_T^+ is the transverse tensile and τ_T the transverse shear strengths and a compressive matrix mode

$$\frac{1}{\sigma_T^-}\left[\left(\frac{\sigma_T^-}{2\tau_T}\right)^2 - 1\right](\sigma_{22} + \sigma_{33}) + \frac{1}{4\tau_T^2}(\sigma_{22} + \sigma_{33}) + \frac{1}{\tau_T^2}(\sigma_{23}^2 - \sigma_{22}\sigma_{33}) + \frac{1}{\tau_A^2}(\sigma_{12}^2 + \sigma_{13}^2) = 1, \tag{19}$$

where σ_T^- is the transverse compressive strength.

The resulting three-dimensional failure surface in a principal stress space illustrated in Fig. 7(a) has the appearance of a parabolic cylinder capped by two parallel planes. By (14) and because (15) does not involve σ_{11}, the fiber mode necessarily reduces to a maximum principal stress condition [Fig. 7(b)] in a principal stress space. The implication of such a failure bound is that lamina consisting of uniaxial fibers would fail by maximum principal stress. However, this is not confirmed by experiment. In the transverse plane, the failure envelope is the union (not the intersection) of areas of both the matrix tensile and

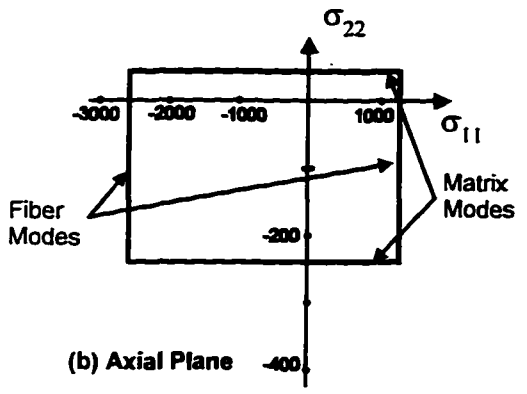

σ^-_{tan} = -240 MPa σ^-_{axl} =-2600MPa

σ^+_{tan} = 45 MPa σ^+_{axl} = 1300MPa

τ_{tan} = 55MPa

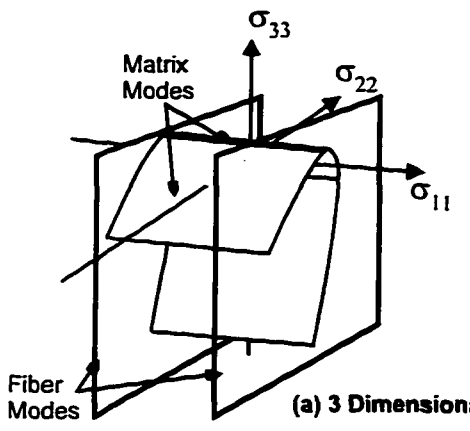

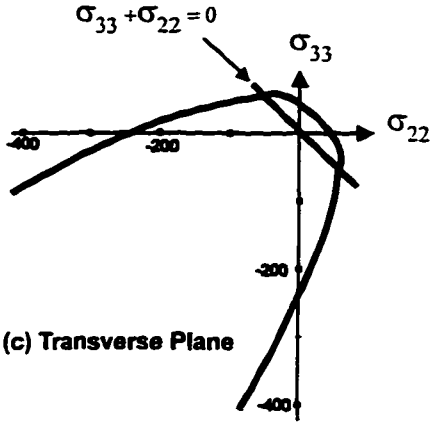

Fig. 7 (a) A plot of the three-dimensional failure surface for a transversely isotropic material as describe by Hashin (1980). The surface has the appearance of a parabolic cylinder capped by two parallel planes. (b) The intercept of the failure envelope with the (σ_{11}, σ_{22}) principal stress plane. Notice that the fiber and matrix failure modes necessarily reduce to a maximum principal stress criterion in this plane. (c) The failure in the (σ_{22}, σ_{33}) plane exhibits a concavity at the $\sigma_{22}+\sigma_{33}=0$ line intercept and does not limit biaxial compressive stress (σ_{22}, σ_{33}).

compressive curves [Fig. 7(c)].Though it is clear that the intention of such a process was to produce two elliptical cross-sections, the matrix compressive mode is not such a curve. It can be shown that (19) is the equation of a parabolic cylinder which displays no bound in biaxial compression. This point, not discussed by the author, is clearly an oversight. Furthermore, though the arguments used to ignore stress interaction terms involving both matrix and fiber modes may, perhaps, be acceptable for the transversely isotropic material considered by the author, it is difficult to see how this same procedure can be applied to any

other type of material symmetry. Indeed orthotropic or even completely anisotropic materials would certainly not be so accommodating.

3.2.2 Modal Decomposition by Strain Invariants (Feng, 1991)

A failure criterion for transversely isotropic composite materials based upon the strain invariants was introduced by Feng (1991). This criterion is assumed to be a function of the strain invariants J_k (where k=1,..,5 for transverse isotropy) such that

$$\begin{aligned} f(J_1,J_2,J_3,J_4,J_5) &= 0, \\ A_1J_1 + A_{11}J_1^2 + A_2J_2 + A_4J_4 + A_5J_5 + A_{55}J_5^2 + A_{15}J_1J_5 - 1 &= 0, \end{aligned} \tag{20}$$

where the A terms are constants to be determined experimentally. If the A_{15} term is assumed to be zero then this criterion can be decoupled into two modes; a matrix dominated mode

$$A_1J_1 + A_{11}J_1^2 + A_2J_2 - 1 = 0 \tag{21}$$

and a fiber dominated one

$$A_5J_5 + A_{55}J_5^2 + A_4J_4 - 1 = 0. \tag{22}$$

Feng(1989) gives the infinitesimal strain invariants as

$$\begin{aligned} J_1 &= \epsilon_{11}+\epsilon_{22}+\epsilon_{33}, \\ J_2 &= \frac{1}{6}\left[(\epsilon_{11}-\epsilon_{22})^2+(\epsilon_{22}-\epsilon_{33})^2+(\epsilon_{33}-\epsilon_{11})^2\right]+\epsilon_{12}^2+\epsilon_{23}^2+\epsilon_{13}^2, \\ J_4 &= \epsilon_{12}^2+\epsilon_{13}^2, \\ J_5 &= \epsilon_{11}. \end{aligned}$$

So that, in terms of the infinitesimal strains the matrix mode criterion is

$$A_1\epsilon_{11}+\epsilon_{22}+\epsilon_{33} + A_{11}\left(\epsilon_{11}+\epsilon_{22}+\epsilon_{33}\right)^2 + A_2\left(\frac{1}{6}\left[(\epsilon_{11}-\epsilon_{22})^2+(\epsilon_{22}-\epsilon_{33})^2+(\epsilon_{33}-\epsilon_{11})^2\right]+\epsilon_{12}^2+\epsilon_{23}^2+\epsilon_{13}^2\right) - 1 = 0 \quad (24)$$

and the fiber mode is

$$A_5\epsilon_{11} + A_{55}\epsilon_{11}^2 + A_4\left(\epsilon_{12}^2+\epsilon_{13}^2\right) - 1 = 0. \quad (25)$$

The failure is prescribed to occur when the magnitude of one of these two modes is exceeded.

Though the author did not plot the failure surface in a principal stress space, it is clear that this procedure should, with the same failure data, produce a similar failure surface as in Hashin and therefore would exhibit the same weaknesses.

3.2.3 Modal Decomposition by Projection operators (Kelvin modes)

Using the foundation provided by Mehrabadi and Cowin (1990), Biegler and Mehrabadi (1993,1995) present a generalization of the von Mises plasticity theory for anisotropic materials. In a later study Schreyer and Zuo (1995) used the same spectral decomposition of the elasticity tensor described by Biegler and Mehrabadi (1993) to produce yield surfaces based on projection operators. It can be shown that the projection operators described by Schreyer and Zuo (1995) are the modal tensors described by Biegler and Mehrabadi (1993, 1995). Thus both approaches result in the same yield surfaces. The formulation for these failure criteria is based upon using the spectral decomposition of the six dimensional elasticity tensor $C_{\alpha\beta}$ such that

$$C_{\alpha\beta} = \sum_{A=1}^{K} \Lambda_A P_{\alpha\beta}^{(A)}, \tag{26}$$

where K ($K \leq 6$) is the number of distinct eigenvalues Λ_A and $P_{\alpha\beta}^{(A)}$ are the modal tensors (Mehrabadi and Cowin, 1990). The number of distinct eigenvalues governs the number of modal tensors $P_{\alpha\beta}^{(A)}$ for a given symmetry.

The stresses T_α and strains E_α may thus be decomposed into K eigenstresses $T_\alpha^{(A)}$ and eigenstrains $E_\alpha^{(A)}$ such that

$$\begin{aligned} T_\alpha^{(A)} &= P_{\alpha\beta}^{(A)} T_\beta, \\ E_\alpha^{(A)} &= \frac{1}{\Lambda_A} T_\alpha^{(A)}, \qquad (\alpha,\beta = 1,...,6,\ A = 1,..,K). \end{aligned} \tag{27}$$

The strain energy U may therefore also be decomposed into the sum of *modal* energies $U^{(A)}$ so that

$$2U^{(A)} = T_\alpha^{(A)} E_\alpha^{(A)} = \frac{1}{\Lambda_A} T_\alpha^{(A)} T_\alpha^{(A)} = \frac{1}{\Lambda_A} P_{\alpha\beta}^{(A)} T_\beta \; P_{\alpha\beta}^{(A)} T_\beta \quad (\alpha = 1,...,6,\ A = 1,...,K) \tag{28}$$

Once these energy modes have been defined for a given material, the threshold values are determined from uniaxial tests. Failure is predicted to occur when the energy stored in any one of these domains reaches a critical value. Both Biegler and Mehrabadi (1993) and Schreyer and Zuo (1995) point out that the method produces failure bounds in a manner completely analogous to von Mises plasticity. In fact the isotropic case for this modal failure theory produces two distinct eigenvalues and thus two modes of failure: a dilatational mode (or a maximum hydrostatic stress failure) and an isochoric shear mode (a maximum

distortional energy or maximum octahedral or von Mises stress).

A comparison of the experimental data for paperboard (Suhling *et al.*, 1985) and the predictions of the modal failure analysis for tetragonal symmetry was provided by Biegler and Mehrabadi (1993) and later again by Martin (1994). The procedure employed in these two studies uses a protocol of active regions to fit the different compressive and tensile strengths to the modal lines illustrated in Fig. 8. The premise of this active regions protocol is that the quadrants of principal stress determine whether a particular mode is active and must be considered or is not and can be ignored. Unfortunately the arguments used to justify this protocol cannot be extended to three dimensions.

Yet in spite of the problems of the active regions protocol, the resulting 2D Failure envelope is intuitively appealing. Though the failure bounds differ somewhat from the experimental data in the biaxial tensile domain, they fit particularly well in the biaxial compressive region. The modes clearly describe the corner which appears in the biaxial compression experimental data. Not only does this corner lend credibility to the concept of modes of failure but also to the premise that these rectilinear bounds are produced from the intercept of the modal failure planes with this biaxial stress plane.

This theory will be the basis for a proposed study of modal failure. The thesis will show how, while dispensing with the active region protocol, the determination of the three-dimensional Kelvin failure modes may be formalized. The study will also reveal a flaw in this failure theory and show how this flaw may be redressed by the introduction of a set of complementary failure modes.

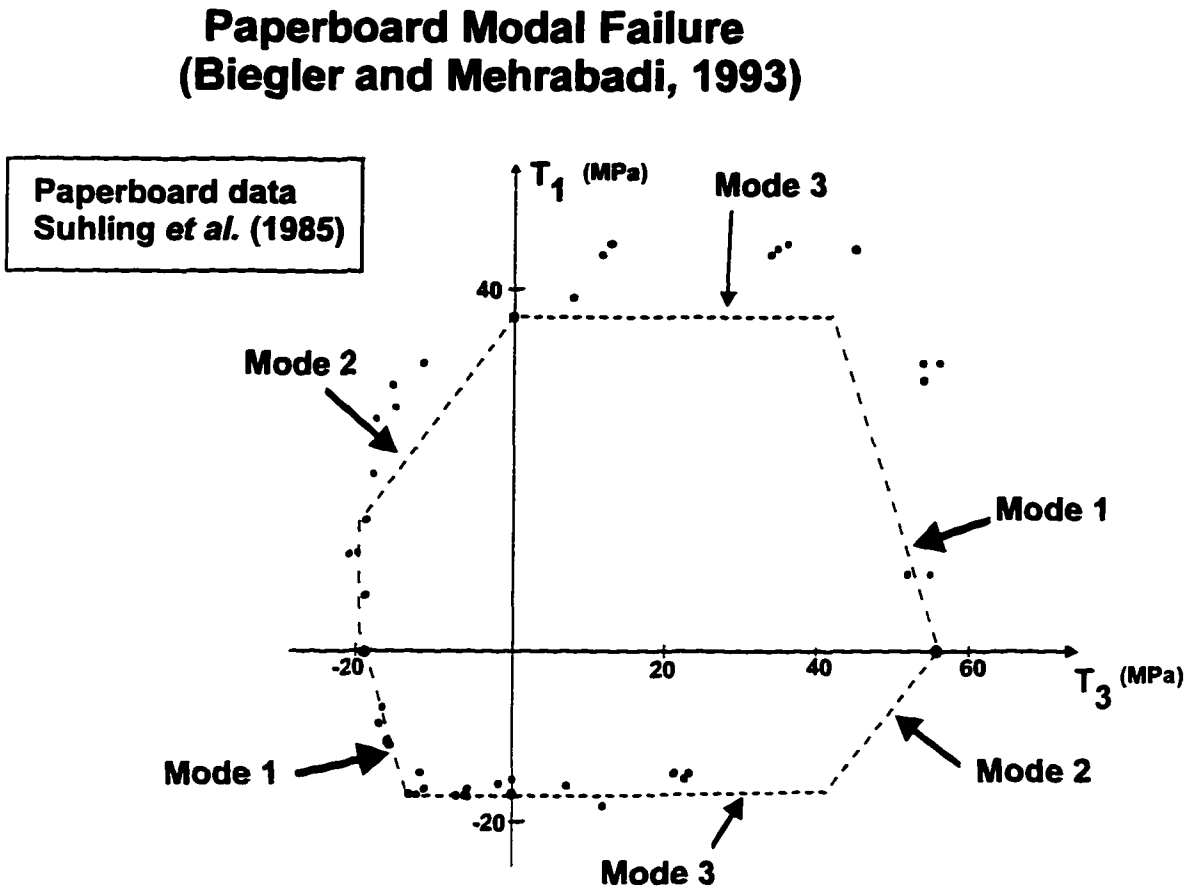

Fig. 8 Plot of the failure envelope as described by Biegler and Mehrabadi (1993) and Martin (1994). The experimental failure data for paperboard (Suhling *et al.*, 1985) is superposed. The quadrants of the principal stress plane define regions where specific modes are (or are not) active. Notice the fit of the corner in the biaxial compression region. The experimental data suggest that this corner does indeed exist and that it is formed by the intersection of two virtually rectilinear bounds.

4 A REVISED MODAL FAILURE THEORY

The procedure employed by Biegler and Mehrabadi (1993) and later again by Martin (1994) to fit the paperboard failure data of Suhling *et al.* (1985) proved to be inapplicable in a three-dimensional stress space. The intent of the active regions protocol described earlier was to accommodate the different tensile and compressive strengths of paperboard. However such a protocol may be dispensed with by observing that the planes of constant modal energy

are also planes of constant eigenstress. Recall that the modal energies are related to the eigenstresses by (28). Suppose Λ_A is distinct (multiplicity of 1). Then (28) can be rewritten as

$$2\Lambda_A U^{(A)} = T_\alpha^{(A)} T_\alpha^{(A)} = \left[\sigma^{(A)} N_\alpha^{(A)}\right]\left[\sigma^{(A)} N_\alpha^{(A)}\right] = \left(\sigma^{(A)}\right)^2 \qquad (\alpha = 1,...,6,\ A = 1,...,K). \tag{29}$$

where $N_\alpha^{(A)}$ is the eigenvector associated with Λ_A and the scalar $\sigma^{(A)}$ is the magnitude of the eigenstress. Using (28) we find that an alternate form for (29) is one which is analogous to the projection operators criterion of Schreyer and Zuo (1995)

$$2\Lambda_A U^{(A)} = P_{\alpha\beta}^{(A)} T_\alpha T_\beta = \left(\sigma^{(A)}\right)^2 \qquad (\alpha = 1,...,6,\ A = 1,...,K). \tag{30}$$

Borrowing the concept from Hashin (1980) that the failure must be evaluated for compressive and tensile modes separately, we presume that the maximum modal energies must be evaluated for compressive and tensile eigenstresses $\sigma^{(A)}$ separately. Thus we obtain two criteria

$$2\Lambda_A U_T^{(A)} = \left(\sigma_T^{(A)}\right)^2 \text{ and } 2\Lambda_A U_C^{(A)} = \left(\sigma_C^{(A)}\right)^2. \tag{31}$$

These conditions define the extreme bounds of the Kelvin mode (A) in stress space. Ideally, the tensile and compressive eigenstress magnitudes $\sigma_T^{(A)}$ and $\sigma_C^{(A)}$ should be determined from a triaxial test. In lieu of such tests, however, these bounds may be estimated from whatever failure data is available. An illustration of how these bounds would be

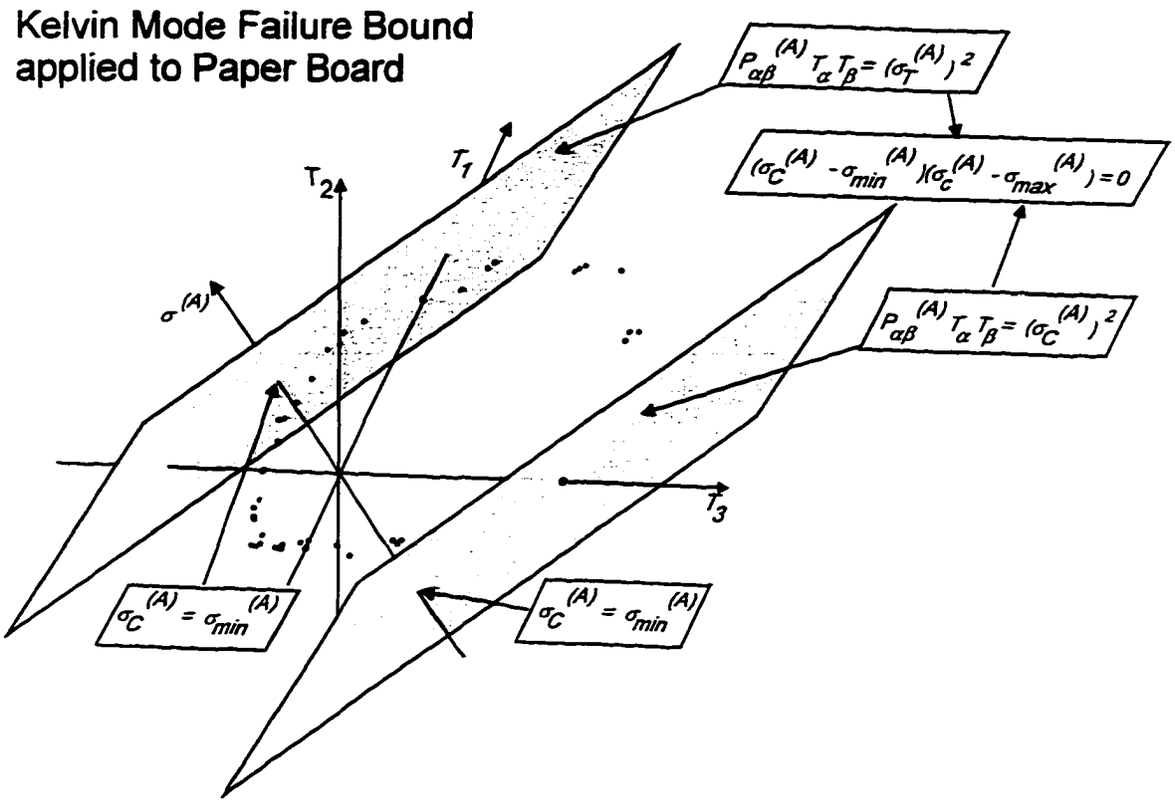

Fig. 9 Illustration of how the compressive and tensile modal bounds are determined. The failure data plotted here is the same paperboard biaxial data as in Fig 8. The two modal energy bounds $P^{(A)}_{\alpha\beta} T_\alpha T_\beta = (\sigma^{(A)}_{min})^2$ and $P^{(A)}_{\alpha\beta} T_\alpha T_\beta = (\sigma^{(A)}_{max})^2$ define maximum and minimum allowable eigenstress magnitudes. Note that, for clarity, although the bounds describe planes in a three-dimensional stress space, only the (T_2, T_3) intercept is shown here.

estimated from the paperboard data is shown in Fig. 9.Given a set of uniaxial and multiaxial strength data, the maximum and minimum eigenstress magnitudes $\sigma^{(A)}_{max}$ and $\sigma^{(A)}_{min}$ can be used estimate $\sigma^{(A)}_T$and $\sigma^{(A)}_C$ and produce K sets of Kelvin modes in the form

$$\left(\sigma^{(A)} - \sigma_T^{(A)}\right)\left(\sigma^{(A)} - \sigma_C^{(A)}\right) = 0, \tag{32}$$

where $\sigma^{(A)}_T = \sigma^{(A)}_{max}$ and $\sigma^{(A)}_C = \sigma^{(A)}_{min}$, A= 1,...,K and K is the number of distinct eigenvalues. For the paperboard example of Biegler and Mehrabadi (1993) and of Martin (1994), this Kelvin mode criterion reduces to a set of three failure criteria given by

$$\underline{\text{KELVIN MODE 1}}$$
$$(\sigma^{(1)} - 47.1)(\sigma^{(1)} + 16.8) = 0, \quad \text{where } \sigma^{(1)} = 0.382(T_1 + T_2) + 0.841 T_3,$$
$$\underline{\text{KELVIN MODE 2}}$$
$$(\sigma^{(2)} - 18.1)(\sigma^{(2)} + 30.3) = 0, \quad \text{where } \sigma^{(2)} = 0.595(T_1 + T_2) - 0.541 T_3, \tag{33}$$
$$\underline{\text{KELVIN MODE 3}}$$
$$(\sigma^{(3)} - 21.6)(\sigma^{(3)} + 9.19) = 0, \quad \text{where } \sigma^{(3)} = \frac{1}{\sqrt{2}}(T_1 - T_2).$$

We therefore obtain two planes for each of the three modes in (33). The reader may refer to section 5.3 for a detailed example of the development of Kelvin modes for biaxial strength data. The resulting failure envelope, illustrated in Fig. 10, is a brick shaped volume. The normal to each face of the brick is a vector in the direction of the eigenstresses. The intercept of this volume with the (T_1, T_3) principal stress plane is entirely consistent with the two-dimensional predictions of Biegler and Mehrabadi (1993) and Martin (1994) described earlier and illustrated in Fig. 8. The advantage that this approaches presents is that it dispenses with the need for the active region protocol previously mentioned. As in these studies, only the uniaxial test data were considered to produce Fig. 10. Consequentially, some of the failure surfaces intersect on the axes (mode 1 and mode 2 on both the T_1 and T_3 axes of Fig. 10). It is possible but not likely that any one, experimentally determined, strength data represents the simultaneous failure by two or more modes. This mode coincidence is an ambiguity since the failure data in question cannot be attributed to a specific Kelvin mode. Therefore when this situation occurs in the course of evaluating the Kelvin mode failure envelope is it necessary to verify or refute this coincidence by additional data.

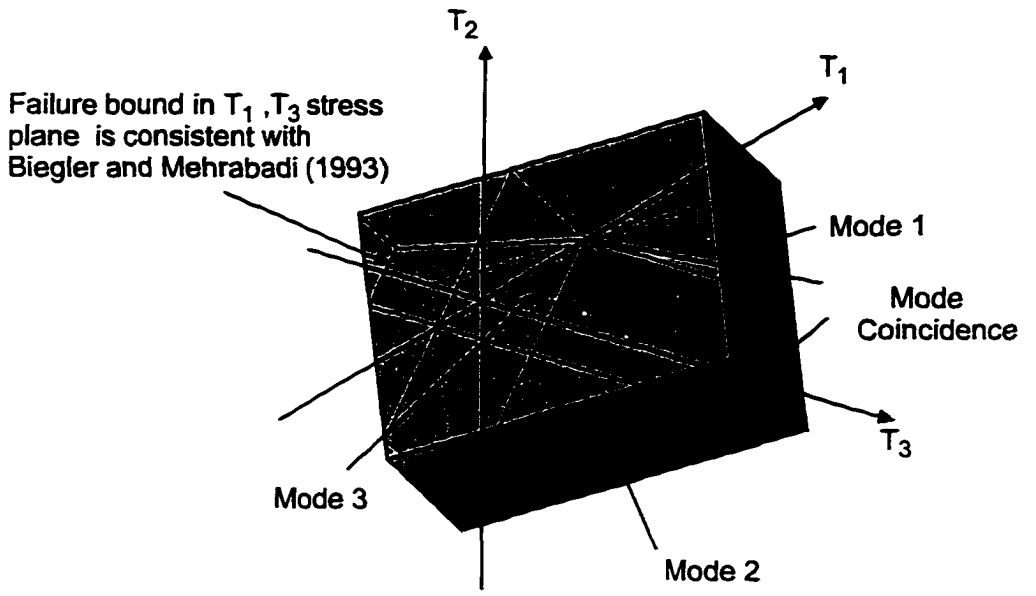

Fig. 10 A 3D plot of the Kelvin mode failure bounds for paperboard. The (T_1, T_3) planar intercept of this failure envelope coincides with the plots produced by Biegler and Mehrabadi (1993) and Martin (1994). Note that this plot was produced with the assumption that only the uniaxial data is available. For this reason Mode 1 and 2 coincide on the T_3 axis and mode 2 and 3 on the T_1 axis. This would not necessarily be the case if the full set of biaxial data were considered.

Ideally, the tensile and compressive eigenstresses should be determined directly from triaxial tests. However triaxial tests are extremely difficult to reproduce accurately so that such data is almost never available. Biaxial data, such as the paperboard data of Suhling *et al.* (1985), is more common and may be used to estimate the bounds on the eigenstresses. Whenever possible the biaxial data from multiple planes should be used. In this case, the biaxial data provided by Suhling *et al.* (1985) is for one plane only (T_1, T_3). However, for the tetragonal symmetry of paperboard it may reasonably be assumed that the strength in the (T_2, T_3) plane is the same as in the (T_1, T_3) plane, so that the intercept of the Kelvin modes with these two stress planes should produce the same predictions. Yet there is no way to accomplish this without introducing a gap in the failure envelope. A plot of the (T_1, T_2) Kelvin modes (Fig. 11) reveals this flaw in the Kelvin mode criterion. If the

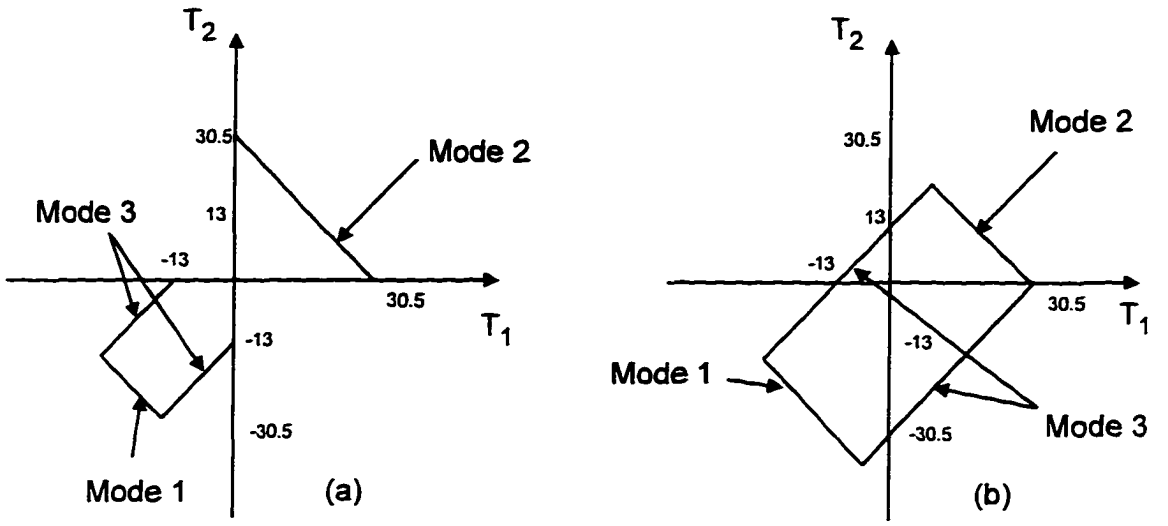

Fig. 11 Illustration of the problem with the (T_1, T_2) Kelvin mode predictions for paperboard strengths. (a) If the tensile/compressive strengths are considered equal, then discontinuities across the axes appear unavoidable. (b) If instead the surfaces are assumed continuous then we have the counterintuitive situation with T_1(comp.) = T_2(tensile) and T_1(tensile) = T_2(comp).

tensile/compressive strengths are considered equal, then discontinuities across the axes appear unavoidable [Fig. 11(a)]. If instead, the surfaces are assumed continuous then the counterintuitive situation arises with T_1(comp.) = T_2(tensile) and T_1(tensile) = T_2(comp.). This problem appears unavoidable and is not unique to this material. Indeed, a similar inconsistency develops when this criterion is applied to elastically isotropic materials like concrete. For isotropy, this modal failure theory reduces the number of modes to two: a distortional (von Mises) and a dilatational (hydrostatic stress) mode. Though the von Mises agrees well with the biaxial compressive data of Kupfer and Gerstle (1973), neither the von Mises nor the maximum hydrostatic stress criteria can account for the failure in the tensile regions (Fig. 12). Clearly, concrete exhibits an additional mode of failure which is unrelated to the Kelvin modes.

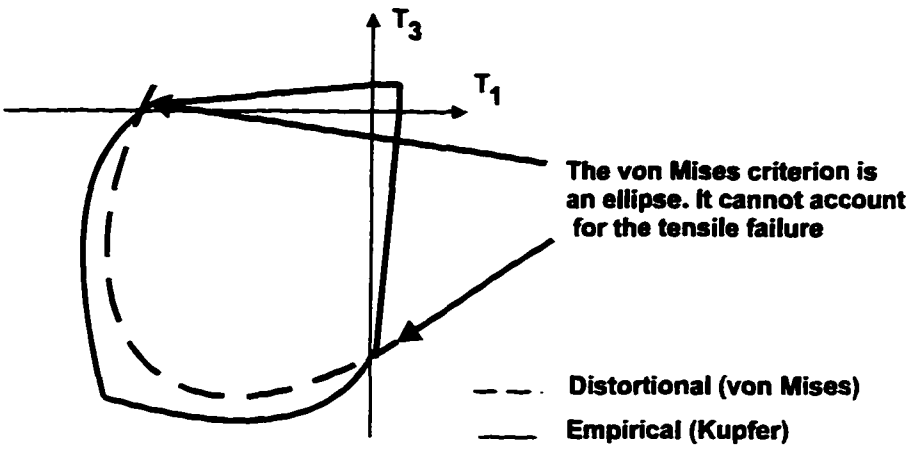

Fig. 12 Illustration of the modal theory's inability to account for the tensile strength of concrete. The empirical curve was produced from experiment (Kupfer and Gerstle, 1973).

These aspects of the modal failure envelope of concrete and paperboard suggest that this criterion provides an incomplete description of the failure.

To accommodate the tensile strength of concrete, it is proposed to revise the Kelvin mode failure theory with the introduction of a set of complementary modes. A set of maximum principal stress modes (or (P) modes) has intuitive appeal and apparently addresses the weaknesses described above. These complementary modes would be determined in a manner analogous to the Kelvin modes, that is to say we define the (P) failure modes such that,

$$\left(\sigma^{(P)} - \sigma_T^{(P)}\right)\left(\sigma^{(P)} - \sigma_C^{(P)}\right) = 0, \tag{34}$$

where $\sigma^{(I)} = T_1$, $\sigma^{(II)} = T_2$ and $\sigma^{(III)} = T_3$. It is important to note that this criterion is not

where $\sigma^{(I)} = T_1$, $\sigma^{(II)} = T_2$ and $\sigma^{(III)} = T_3$. It is important to note that this criterion is not equivalent to a maximum uniaxial stress criterion. Instead, the bounds $\sigma_T^{(P)}$ and $\sigma_C^{(P)}$ are determined from the entire set of uniaxial and multiaxial failure data so that $\sigma_T^{(P)} = \sigma_{max}^{(P)}$ and $\sigma_C^{(P)} = \sigma_{min}^{(P)}$.

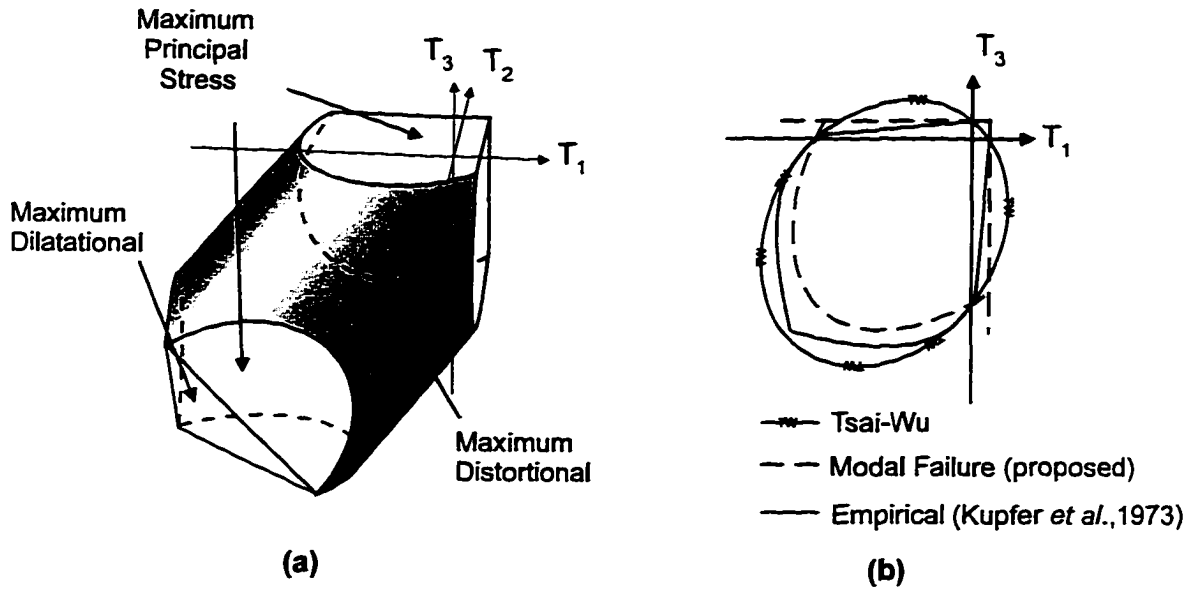

(a) (b)

Fig. 13 (a) A three-dimensional representation of the modified modal failure theory. The envelope has been extended in the compressive region for illustrative purpose. (b) The addition of a complementary maximum principal stress mode produces a failure envelope consistent with the experimental data of Kupfer *et.al.* (1973). The proposed modal criterion fits the experimental data better than the Tsai-Wu for this case.

When this complementary criterion is applied to the concrete failure data [Fig. 13(a)] it produces an intuitively appealing three-dimensional failure envelope which is in agreement with the predictions of Kupfer and Gerstle (1973). Particularly noteworthy is the fact that this revised modal theory succeeds in accounting for the tensile strength of concrete [Fig. 13(b)]. Indeed, an appropriate Tsai-Wu criterion could never account for the discontinuities apparent in the experimental data.

The revised modal theory may therefore be formally described by

$$\left(\sigma^{(A)} - \sigma_T^{(A)}\right)\left(\sigma^{(A)} - \sigma_C^{(A)}\right) = 0, \quad \textit{and} \quad \left(\sigma^{(P)} - \sigma_T^{(P)}\right)\left(\sigma^{(P)} - \sigma_C^{(P)}\right) = 0, \tag{35}$$

where

$\sigma^{(A)}$ is the magnitude of the eigenstress associated with the eigenvalue Λ_A of the material's elasticity tensor,

$\sigma_T^{(A)} = \sigma_{max}^{(A)}$ is the largest value of $\sigma^{(A)}$ that can be determined from the available failure data set,

$\sigma_C^{(A)} = \sigma_{min}^{(A)}$ is the smallest value of $\sigma^{(A)}$ that can be determined from the available failure data set,

A=1,..,K where K is the number of distinct eigenvalues of the material's elasticity tensor,

$\sigma^{(P)}$ is the magnitude of the principal stress (complementary mode)

$\sigma_T^{(P)} = \sigma_{max}^{(P)}$ is the largest value of $\sigma^{(P)}$ that can be determined from the available failure data set,

$\sigma_C^{(P)} = \sigma_{min}^{(P)}$ is the smallest value of $\sigma^{(P)}$ that can be determined from the available failure data set,

When this revised modal theory is applied to the paperboard example it produces six modes of failure: three Kelvin and three complementary modes given by

KELVIN MODE I

$$(\sigma^{(1)} - 47.102861)(\sigma^{(1)} + 16.82245) = 0, \quad \text{where } \sigma^{(1)} = 0.3824349056(T_1 + T_2) + 0.841122515T_3,$$

KELVIN MODE 2

$$(\sigma^{(2)} - 18.140285)(\sigma^{(2)} + 30.28730) = 0, \quad \text{where } \sigma^{(2)} = 0.5947634345(T_1 + T_2) - 0.54084463T_3,$$

KELVIN MODE 3

$$(\sigma^{(3)} - 21.566757)(\sigma^{(3)} + 9.192388) = 0, \quad \text{where } \sigma^{(3)} = \frac{1}{\sqrt{2}}(T_1 - T_2), \tag{36}$$

P MODE I

$$(\sigma^{(I)} - 30.5)(\sigma^{(I)} + 13.0) = 0, \quad \text{where } \sigma^{(I)} = T_1,$$

P MODE II

$$(\sigma^{(II)} - 30.5)(\sigma^{(II)} + 13.0) = 0, \quad \text{where } \sigma^{(II)} = T_2,$$

P MODE III

$$(\sigma^{(III)} - 56.0)(\sigma^{(III)} + 20.0) = 0, \quad \text{where } \sigma^{(III)} = T_3.$$

The revised paperboard failure envelope displays intuitively correct strength prediction in the (T_2, T_3) biaxial stress plane [Fig. 14(b)]. Though not illustrated, the strength prediction in (T_1, T_3) is identical to that in the (T_2, T_3) plane and is therefore consistent with intuition. The complete three-dimensional failure envelope is the intersection of the Kelvin and complementary mode failure volumes [Fig. 14(a)]. There still remains an ambiguity in the (T_1 ,T_2) stress plane [Fig. 14(c)]. The mode coincidence apparent in Fig. 14(c) is due to the lack of biaxial data for this stress plane.

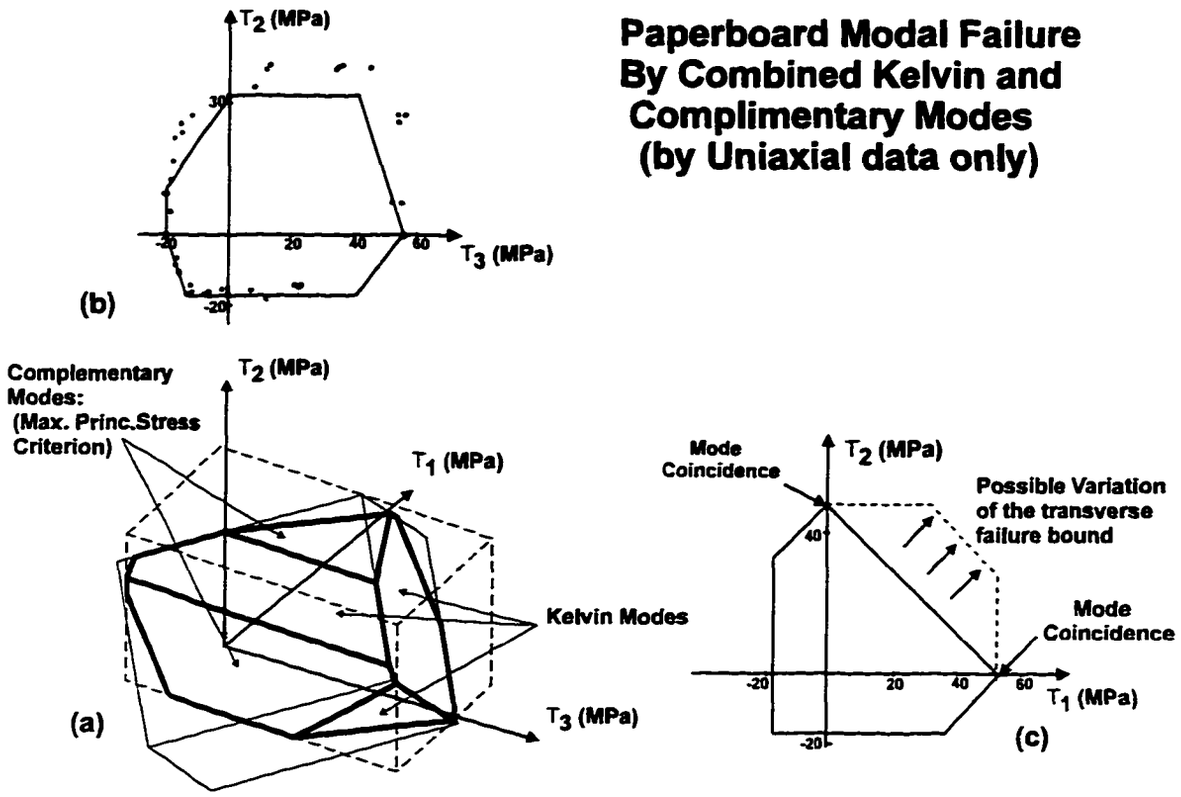

Fig. 14 Illustration of the revised three-dimensional modal failure envelope (a). The Kelvin and complementary modes are superimposed. The intersection of these mode sets is the proposed failure envelope. (b) The trace of the modal failure envelope in the (T_2, T_3) plane is consistent with the results proposed in Biegler and Mehrabadi (1993). Though not illustrated here, the trace in (T_1, T_3) is identical to that in the (T_2, T_3) plane. (c) The trace of the modal failure envelope in the (T_1, T_2) plane. Transverse biaxial data is not available, therefore the (T_1, T_2) failure envelope may still display the variation shown in (c).

To conclude the theoretical development of this revised modal theory the following recapitulation is presented. A new theory for the prediction of strength of anisotropic elastic materials was proposed by Biegler and Mehrabadi (1993). However, the logic employed by these authors to formulate a failure criterion based on this theory could not be extended to multiaxial stress. In this thesis, an alternate criterion was presented which redressed the biaxial restriction by reformulating the surfaces of constant modal energy as surfaces of

constant eigenstress magnitude. The resulting failure envelope, in a multidimensional stress space, is piecewise smooth. Each facet of the envelope is expected to represent the locus of failure data by a particular Kelvin mode. It was further shown that the Kelvin mode theory alone provides an incomplete description of the failure of some materials, but that this weakness can be addressed by the introduction of a set of complementary modes. A revised theory which combines both Kelvin and complementary modes was thus proposed and applied to two examples: the paperboard example used by Biegler and Mehrabadi (1993) and an isotropic concrete. The resulting failure envelopes for these two examples appear to produce intuitively correct failure predictions. In the following sections, this revised theory will be applied to seven engineering examples.

5 APPLICATION OF MODAL FAILURE TO SELECTED MATERIALS

5.1 Determination of the Failure Envelope

There are two sets of data which are critical to the determination of the modal failure envelope for any material: the eigenvectors of the elasticity tensor and the bounds or critical values of the Kelvin and complementary modes.

The Kelvin modes are planes of constant eigenstress. The orientations of these planes are dependant upon the eigenvectors of the material's elasticity tensor. It is critical therefore that these eigenvectors be determined as a first step in the analysis. In most cases, the tensor may be measured by either mechanical testing (Wood Handbook, 1974) or by ultrasound (François, 1995). Occasionally the method of measurement of the elastic constants is dependant upon the physical limitations of the sample that can be excised from the material. For instance, though highly porous materials such as trabecular bone may display macroscopically homogeneous mechanical behavior, they are in fact inhomogeneous. In such cases a judiciously chosen sample size will provide mechanical measurements that are representative of the material. A sample size of five trabecular lengths is believed to be appropriate for trabecular bone (Harrigan *et al.*, 1988). If the material microstructure can be reconstructed as a computer model then either a finite element model or a reconstruction by rapid polymerization may be used to determine an average elastic behavior and the elasticity tensor deduced from it. Some material exhibit a visual indication of the principal directions of its material properties, such as the grain of wood. For such material, a specimen may be shaped in such a way as to accommodate testing in these directions. If the material exhibits no such visual indication then the elasticity tensor may be determined for multiple specimens

and average of the elastic properties may be deduced from the entire set (François, 1995; Cowin and Yang, 1997). Regardless of what method is used the elasticity tensor is central to the theory because it indicates the symmetry of the material and the orientation of the Kelvin modes.

Once the orientations of the modal failure surfaces have been established, their position in principal stress space can be determined. For the isotropic case this would be equivalent to establishing the maximum allowable von Mises stress from the available data. However, unlike the isotropic case, an anisotropic material would require a minimum of six pairs of failure data to establish the maximum Kelvin modes. Fortunately, in a principal stress space this number can be reduced to three pairs of failure data since, in many case, only three modal surfaces can be represented in this stress space. In addition to the Kelvin modes, at least three pairs of failure data are required to establish the maximum complementary modes. This brings the total number of required failure data to six pairs, or twelve test points. Ideally, a succession of three pairs of uniaxial tests followed by three pairs of multiaxial (triaxial) strengths test performed in the direction normal to the Kelvin modes should be performed. These data points would provide a first conservative estimate of the Kelvin mode failure bounds. Following these six triaxial tests, six additional mechanical tests could be performed in the direction least likely to intercept a Kelvin mode failure surface (the directions of which would be apparent from the initial failure envelope). Each consecutive set of data would produce successively less conservative failure envelopes. The failure envelope would be presumed to be completely defined when a sufficient number of failure data points could be uniquely attributed to each failure mode. Among the

numerical examples presented in Sec. 5.2 of this study, triaxial failure data for an isotropic concrete will used to estimate its modal failure envelope.

Unfortunately, a reliable procedure for triaxial testing of anisotropic materials is by no means established. Multiaxial tests are difficult to reproduce accurately even for isotropic materials so it is unlikely that this type of data would be available for anisotropic materials in the near future. It is more reasonable to expect that biaxial data may be available. It is possible to determine the mode bounds from a set of biaxial strength data in mutually orthogonal stress planes. With such data, the position of the failure modes are simply the outermost envelope, one which includes all of the strength data. If the theory is applicable, the data should closely match the envelope created by the Kelvin and complementary modes. To illustrate this method the paperboard data of Suhling *et al.* (1985) used by Biegler and Mehrabadi (1993) is reexamined in sec 5.3. In this case, however, the entire set of biaxial stress data is employed to produce the mode bounds and the resulting envelope reproduced. Though this example lacks biaxial data in the transverse plane, the resulting envelope is almost completely defined and should provide sufficient illustration for this method.
Even biaxial data is difficult to come by. In sec. 5.4 four wood examples are presented. These modal failure envelopes are reproduced from uniaxial strengths alone. Though in generally uniaxial strengths are insufficient for the modal theory, the particularly strong anisotropy of woods has helped produce modal failure envelopes which are restricted in the direction of the grain. Consequentially, it does not appear that these failure envelopes would be significantly affected by the inclusion of biaxial strength data. The final example presented in this thesis is that of cortical bone in sec 5.5. Only uniaxial strength data is

available for this material and the resulting Kelvin mode failure envelope is compare to an available Tsai-Wu.

5.2 Numerical Example: Concrete (Isotropic)

Although isotropic materials are not strictly within the scope of this study, the experimental data of Kupfer and Gerstle (1973) along with the triaxial data (Wang *et al.*, 1987) are true biaxial and triaxial data. This presents an appealing opportunity to validate the concept of a combined Kelvin and modal failure envelope. Furthermore, Wang *et al.* (1987) have reported apparent differences in the failure mechanism. These different types of failure appear to correlate with different orthogonal load ratios. This presents an opportunity which is unmatched by any other available data, whether it be multiaxial or otherwise.

For an isotropic material the total number of Kelvin modes is two. Martin (1979) shows that this theory reduces to the maximum distortional and dilatational energy theory. The distortional mode of failure is equivalent to the von Mises envelope described earlier: a tube oriented with its axis along the median vector in a principal stress space, and the dilatational mode is equivalent to a maximum hydrostatic stress criterion: a plane normal to the same median vector. So that, the modal products are written as

$$\begin{aligned} P^{(1)}_{\alpha\beta} T_\alpha T_\beta &= (T_1 + T_2 + T_3)^2 = (\sigma^{(1)})^2, \\ P^{(2)}_{\alpha\beta} T_\alpha T_\beta &= (T_1 - T_2)^2 + (T_2 - T_3)^2 + (T_1 - T_3)^2 = (\sigma^{(2)})^2. \end{aligned} \tag{37}$$

It should be noted that mixing strength data from two different sources is not rigorously correct. There are several parameters that significantly affect both the strength and the elasticity of concrete such as density, mixing proportions, curing temperature, drying

time and humidity. Furthermore, Kupfer and Gerstle (1973) employed brush bearings to reduce friction between the steel platens of their biaxial testing device, whereas Wang *et al.* (1987) employed fluorine-based (Teflon) sheets one to two millimeters thick for that same purpose. All of these differences may account for the disagreement between the biaxial data of Kupfer and Gerstle (1973) and the nearly biaxial data of Wang *et al.* (1987). Nevertheless, for lack of better data, the resulting combined Kelvin and complementary modes are produced here for both sets of data. A list of the triaxial strength data is omitted here. The reader may refer to Wang *et al.* (1987) for a complete report of this data. Only the final results are reported for this example. Thus the modal failure envelope for concrete may be written in the same form as (35). Thus the two Kelvin modes are,

Kelvin Mode 1

$$\begin{gathered}\left(\sigma^{(1)}-0.346\right)\left(\sigma^{(1)}+8.13\right)=0,\\ \text{where } \sigma^{(1)}=T_1+T_2+T_3,\end{gathered} \tag{38}$$

Kelvin Mode 2

$$\begin{gathered}\left(\sigma^{(2)}-47.1\right)\left(\sigma^{(2)}+47.1\right)=0,\\ \text{where } \sigma^{(2)}=\sqrt{\left(T_1-T_2\right)+\left(T_2-T_3\right)+\left(T_3-T_1\right)}.\end{gathered} \tag{39}$$

It should be noted that the distortional mode for this symmetry the same distortional tube illustrated in Fig. 2 (b) and therefore $\sigma^{(2)}$ does not exhibit positive and negative values. Nevertheless the criterion may always be written in the same form as (35).

The complementary principal modes are simply the extreme values of tensile and compressive stress. So that,

Principal Mode 1, 2 and 3

$$\begin{gathered}(\sigma^{(i)} - 0.2)(\sigma^{(i)} + 8.3) = 0, \\ \text{where } \sigma^{(i)} = T_i, \text{ and where } i = 1,2,3\end{gathered} \tag{40}$$

The resulting three-dimensional failure envelope [Fig. 15(a)] appears to be much wider than anticipated. The intercept of the distortional Kelvin mode 2 produces a biaxial trace which is counterintuitive [Fig. 15(b)]. The modal failure envelope cannot account for the uniaxial strengths in any direction. The explanation for this result is apparent when comparing the predictions of the von Mises failure surface with the empirical relationships of concrete triaxial strength suggested by Hobbs (1974), Richart (Newman 1971) and Newman (1971). The particular triaxial data graphed in Fig. 16 is such that the T_1 strength is plotted against a combined lateral stress T_2=T_3, where all stresses are normalized to the uniaxial strength. Both empirical curves exhibit a much greater slope than the von Mises criterion. This suggests that concrete, when constrained by a small lateral load, is much stronger than the von Mises criterion would predict. Consequentially, the distortion at triaxial failure is much higher than at uniaxial failure. This result is, in retrospect, not entirely unexpected. There are several reasons why these results differ so much from the distortional mode predictions. It is unclear whether the Teflon sheet used by Wang *et al.* (1987) to reduce the friction between the platen and concrete surface was effective. The boundary conditions may have introduced an artificially high triaxial strength. This effect would presumably be much more apparent at near uniaxial strength. This is precisely where it occurs in the data. Other investigators have employed various friction reducing methods such as the brush-bearing platens used by Kupfer and Gerstle (1973). Nevertheless, the effect of

lateral friction appears to have been of great concern to these investigators.

A particular aspect of aggregate mechanical behavior is the packing of the material subjected to compressive loads. This packing induces changes in the elastic behavior of concrete. Kupfer and Gerstle (1973) recognized this and adjusted their von Mises based empirical curve to accommodate the increased stiffness at near failure stress levels. More problematic is the possibility that combined compressive stresses may have introduced changes in the symmetry of the aggregate. Indeed, Wang *et al.* (1987) report variation of failure mechanisms over the range described by the empirical curves in Fig. 16. The *postmortem* appearance of the samples varies from column-shaped cracks when $T_2 = T_3 < 0.1 * T_1$ (i.e., $T_1 < 2$) to slice-shaped cracks when $T_2 = T_3 > 0.2 * T_1$ (i.e., $T_1 > 5$). In this case the material may not have been isotropic at all at near failure stress and, therefore, the von Mises theory would be invalid. This may explain the deviation of the triaxial data of

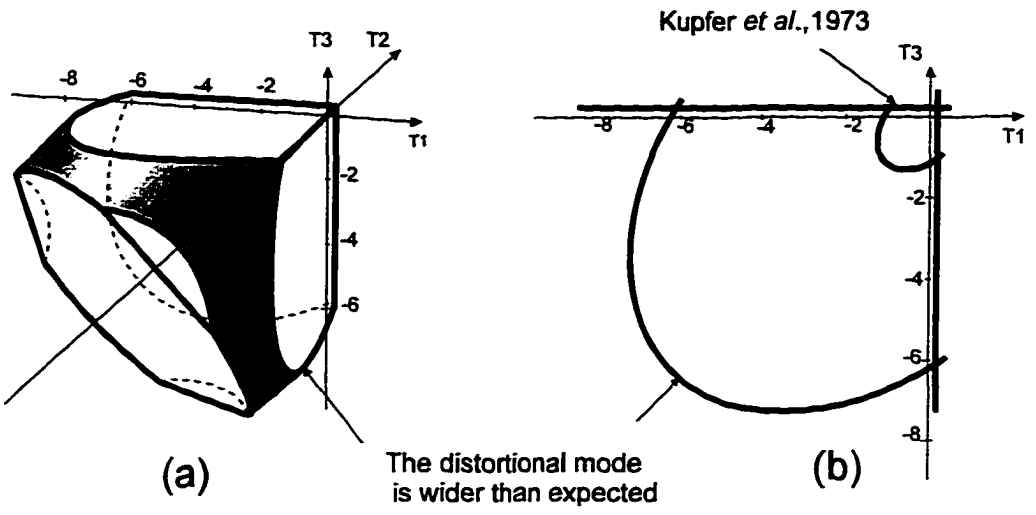

Fig. 15 (a) Plot of three-dimensional modal failure envelope for concrete using available triaxial strength data. (b) The biaxial trace of the modal theory plotted with the prediction of Kupfer and Gerstle (1974).

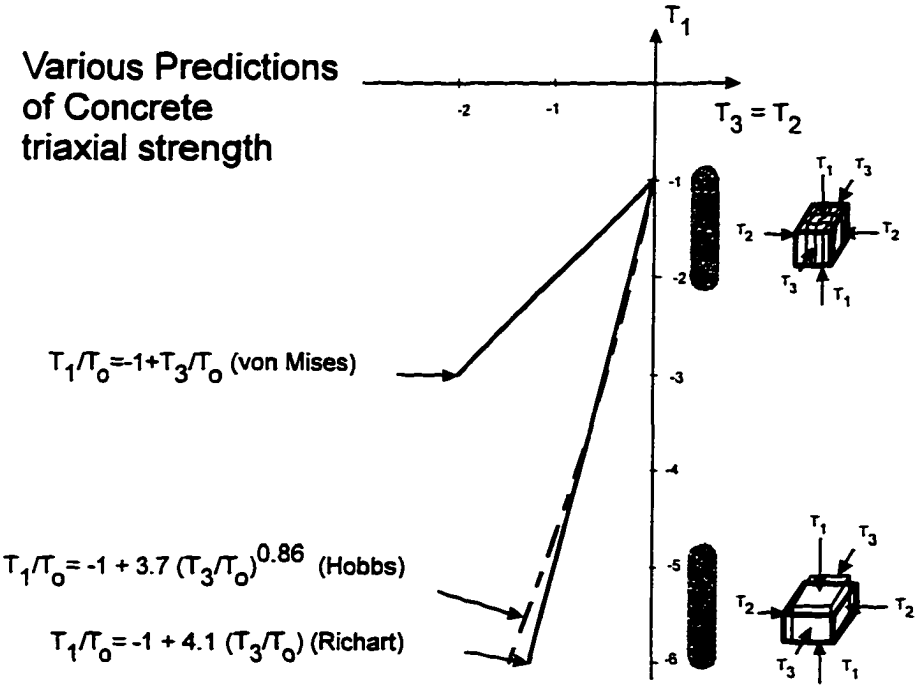

Fig. 16 Plot of two empirical predictions of concrete triaxial strength. The plot illustrates the reason why the distortional mode is wider than expected. The von Mises curve exhibits a lesser slope than the strength data.

Wang *et al.* (1987) from the von Mises predictions. This example illustrates the importance of identifying what the type of failure this criterion is meant to describe. Implicit in the development of the modal criterion is the expectation that the material remains linearly elastic within the failure envelope. However, with reported strains at failure of 20 to 30% (Wang *et al.*, 1987), this was certainly not the case for these experimental data.

5.3 Numerical Example: Paperboard (Tetragonal) with biaxial data

The following is a description of the calculations and assumptions for a three-dimensional representation of the failure bounds for the same paperboard example illustrated in Fig. 14 but with the inclusion of available biaxial strength data (Suhling *et al.*, 1985). The elastic constants for cardboard, as given by Martin (1994), are

E_1=3510 MPa E_2=3510 MPa E_3=6930 MPa

ν_{13}=0.15 ν_{23}=0.15 ν_{12}=0.3

G_{23}=1700 MPa G_{13}=1700 MPa G_{12}=1500 MPa

The paperboard elasticity tensor is deduced from the elasticity data listed above:

$$\boldsymbol{C} = \begin{bmatrix} 4.22E+3 & 1.52E+3 & 1.70E+3 & 0 & 0 & 0 \\ 1.52E+3 & 4.22E+3 & 1.70E+3 & 0 & 0 & 0 \\ 1.70E+3 & 1.70E+3 & 7.94E+3 & 0 & 0 & 0 \\ 0 & 0 & 0 & 1.70E+3 & 0 & 0 \\ 0 & 0 & 0 & 0 & 1.70E+3 & 0 \\ 0 & 0 & 0 & 0 & 0 & 1.50E+3 \end{bmatrix} \cdot \text{MPa} . \quad (41)$$

The eigenvalues for this tetragonal symmetry are given as,

$$\Lambda = \begin{bmatrix} 9.48E+3 \\ 4.2E+3 \\ 2.7E+3 \\ 1.7E+3 \\ 1.7E+3 \\ 1.5E+3 \end{bmatrix} \cdot \text{MPa} , \tag{42}$$

and the corresponding eigenvectors are

$$N1 = \begin{bmatrix} 0.382435 \\ 0.382435 \\ 0.841123 \\ 0 \\ 0 \\ 0 \end{bmatrix}, N2 = \begin{bmatrix} -0.594763 \\ -0.594763 \\ 0.540845 \\ 0 \\ 0 \\ 0 \end{bmatrix}, N3 = \begin{bmatrix} -0.7071068 \\ 0.7071068 \\ 0 \\ 0 \\ 0 \\ 0 \end{bmatrix}, N4 = \begin{bmatrix} 0 \\ 0 \\ 0 \\ 1 \\ 0 \\ 0 \end{bmatrix}, N5 = \begin{bmatrix} 0 \\ 0 \\ 0 \\ 0 \\ 1 \\ 0 \end{bmatrix}, N6 = \begin{bmatrix} 0 \\ 0 \\ 0 \\ 0 \\ 0 \\ 1 \end{bmatrix} \tag{43}$$

The first three modal products are then given by (29)

$$\begin{aligned} P^{(1)}_{\alpha\beta} T_\alpha T_\beta &= \left(0.382(T_1+T_2)+0.841T_3\right)^2 = (\sigma^{(1)})^2, \\ P^{(2)}_{\alpha\beta} T_\alpha T_\beta &= \left(0.595(T_1+T_2) - 0.541T_3\right)^2 = \left(\sigma^{(2)}\right)^2, \\ P^{(3)}_{\alpha\beta} T_\alpha T_\beta &= \left(0.707*(T_1-T_2)\right)^2 = \left(\sigma^{(3)}\right)^2. \end{aligned} \tag{44}$$

The last three modal product reduce to maximum shear stress criteria

$$\begin{aligned} P^{(4)}_{\alpha\beta} T_\alpha T_\beta &= (T_4)^2 = (\sigma^{(4)})^2, \\ P^{(5)}_{\alpha\beta} T_\alpha T_\beta &= (T_5)^2 = (\sigma^{(5)})^2, \\ P^{(6)}_{\alpha\beta} T_\alpha T_\beta &= (T_6)^2 = (\sigma^{(6)})^2. \end{aligned} \tag{45}$$

These last three modes do not involve T_1, T_2, or T_3 and therefore have no meaningful representation in this principal stress space.

In this case the entire biaxial strength data is included in the evaluation of the modal failure envelope. The data was interpreted from the biaxial strength plot in Martin (1994) for the same paperboard data studied by Suhling *et al.* (1985). This strength data along with the Kelvin mode magnitudes are tabulated in the Appendix (table 7).

Then by (32) the three Kelvin modes become

Kelvin Mode 1

$$\begin{aligned} &\left(\sigma^{(1)} - 47.1\right)\left(\sigma^{(1)} + 16.8\right) = 0 \\ &\text{where } \sigma^{(1)} = \left(0.382(T_1 + T_2) + 0.841 T_3\right) \end{aligned} \tag{46}$$

Kelvin Mode 2

$$\begin{aligned} &\left(\sigma^{(2)} - 18.1\right)\left(\sigma^{(2)} + 30.3\right) = 0, \\ &\text{where } \sigma^{(2)} = 0.595(T_1 + T_2) - 0.541 T_3. \end{aligned} \tag{47}$$

Kelvin Mode 3

$$\begin{aligned} &\left(\sigma^{(3)} - 21.6\right)\left(\sigma^{(3)} + 9.19\right) = 0, \\ &\text{where } \sigma^{(3)} = 0.707(T_1 - T_2). \end{aligned} \tag{48}$$

These Kelvin modes are equations of parallel planes in principal stress space (T_1, T_2, T_3) and, along with the maximum stress planes, represent the failure bounds in this space. The resulting three-dimensional modal failure envelope is illustrated in Fig. 17(a). Although the difference between Fig. 17(a) and Fig. 14(a) may not be obvious, it is much more discernable between the (T_3-T_2) biaxial intercept of both failure envelopes [Fig. 14(b) and Fig. 17 (b)]. The improvement in the biaxial tensile strength predictions is entirely due to the inclusion of the biaxial strength in the determination of this modal failure envelope. Although not plotted in this study, the (T_1-T_3) trace is identical to that of the (T_3-T_2) biaxial

stress plane. The fit of biaxial strength experimental data is unusually good. The predictions of the modal failure theory appear to account for the particularities of the strength distribution in every region. The biaxial compressive strength is consistent with the intersection of a Kelvin mode 1 and a complementary mode. The combined T_2 (tensile) and T_3 (compressive) strength prediction also appears to be consistent with the intersection of a Kelvin mode 2 and a complementary mode. Of course the lack of biaxial transverse strength is apparent in the (T_1-T_2) biaxial trace [Fig. 17 (c)]. If such data were available, the trace in this plane may have a somewhat different appearance.

A comparison of the biaxial modal failure predictions with an appropriate Tsai-Wu envelope (Suhling *et al.*, 1985) is illustrated in Fig. 18. The modified modal theory appears to fit the experimental data even better than the Tsai-Wu suggested by Suhling *et al.* (1985).

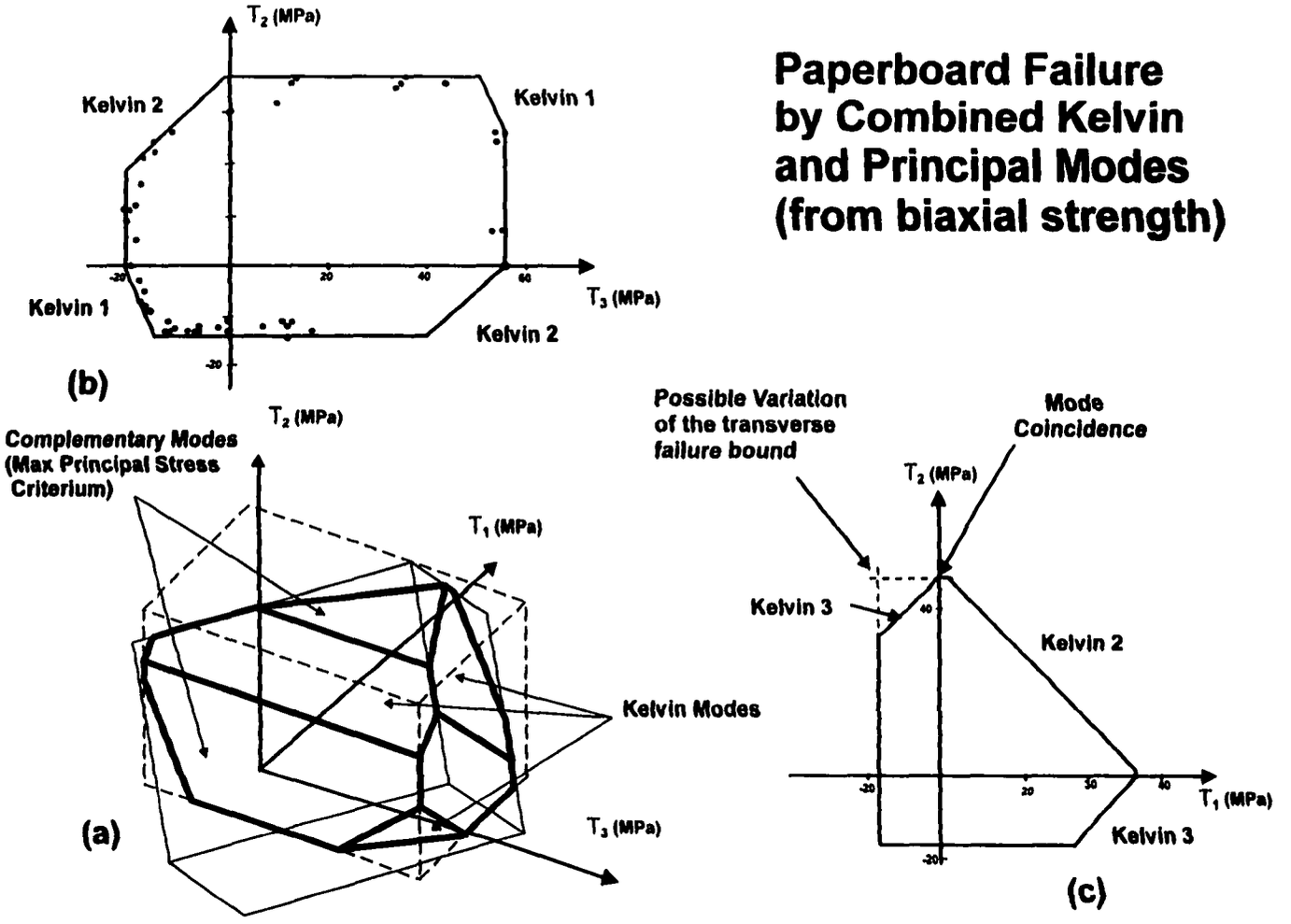

Fig. 17 Illustration of the revised three-dimensional modal failure envelope (a). The Kelvin and complementary modes are superimposed. The intersection of these mode sets is the proposed failure envelope. (b) The trace of the modal failure envelope in the (T_2, T_3) plane is consistent with the results proposed in Biegler and Mehrabadi (1993) . Though not illustrated here the trace in (T_1, T_3) is identical to that in the (T_2, T_3) plane. (c) The trace of the modal failure envelope in the (T_1, T_2) plane. Transverse biaxial data is not available, therefore the (T_1, T_2) failure envelope may still display the variation shown in (c).

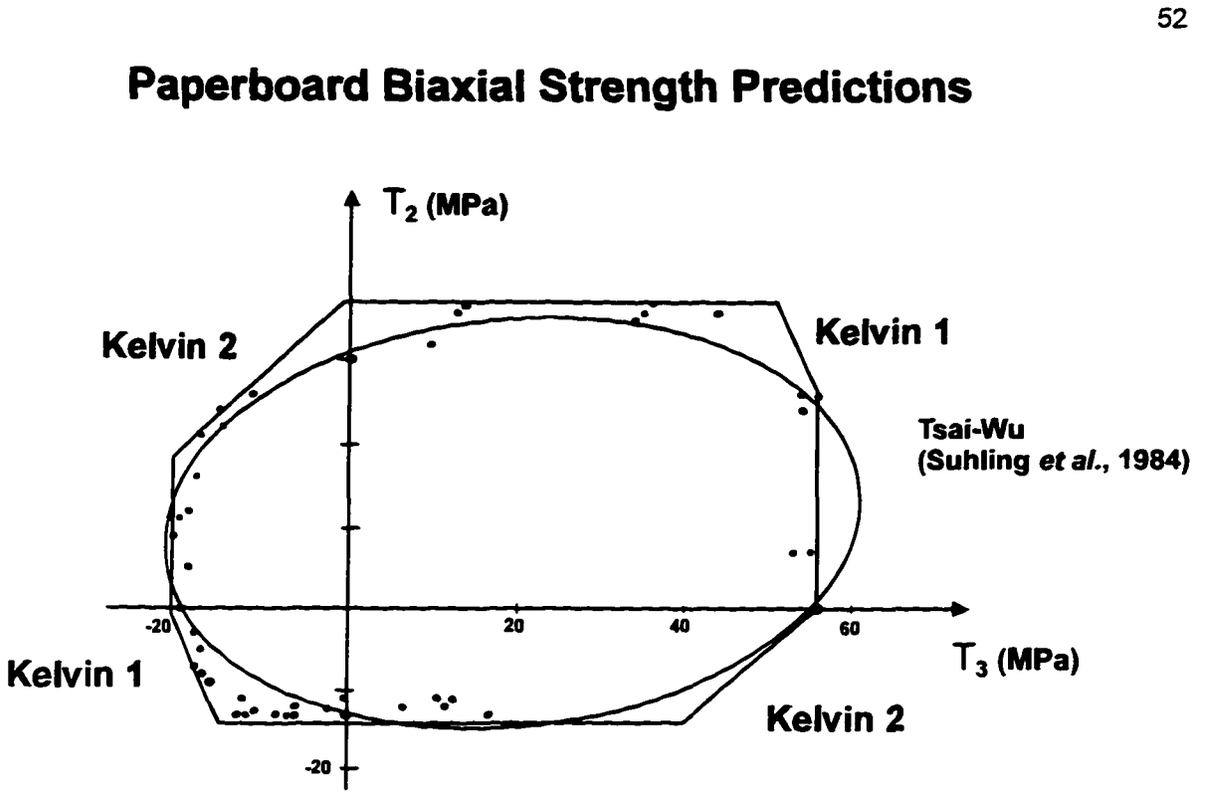

Fig. 18 Comparison of the biaxial modal failure predictions with an appropriate Tsai-Wu envelope (Suhling *et al.*, 1985). The Tsai-Wu coefficients are F_1=-4.4E-2 MPa^{-1}, F_{11}= 2.5E-3 MPa^{-2}, F_3= -3.2E-2MPa^{-1}, F_{33}= 8.9E-4MPa^{-2} and the stress interaction term is determined using the relationship developed by (Cowin, 1979) that is: F_{13}= -3.3E-4 MPa^{-2}. The modal failure theory appears to fit this experimental data better than the suggested Tsai-Wu.

5.4 Four Woods (Orthotropic)

The modal failure envelope for two softwoods (Spruce Sitka, Douglas fir) and two hardwoods (Northern red Oak, yellow Birch) are presented here. Some of the elasticity tensors were obtained from (François, 1995) while others were deduced from the engineering constants tabulated in the Wood Handbook (1974).

For orthotropic materials, only the first three Kelvin modes have representations in principal stress space whereas the last three reduce to maximum shear criteria with no components in principal stress space. If one could picture a six dimensional surface, these last modes would appear as surfaces parallel to principal stress space, never intercepting it.

No multiaxial data was found for these woods. Only the uniaxial strength along and across the grain is reported. Thus the radial and tangential strengths are assumed equal for each of the four wood examples.

5.4.1 Numerical example: (Softwood) Douglas Fir

The engineering constants for Douglas Fir were reported by Schniewind (1979) as,

$E_1 = 670$ MPa	$E_2 = 13400$ MPa	$E_3 = 911$ MPa
$\nu_{13} = 0.29$ (+0.001)	$\nu_{23} = 0.29$	$\nu_{12} = 0.02$ (+0.002)
$\nu_{31} = 0.39$ (+0.005)	$\nu_{32} = 0.02$	$\nu_{21} = 0.45$
$G_{23} = 858$ MPa	$G_{13} = 94$ MPa	$G_{12} = 1045$ MPa

where indices 1, 2, 3 represent the tangential, longitudinal and radial direction respectively and where the values in parentheses are adjustments made to accommodate the symmetry of the compliance and elasticity tensor. The stiffness tensor is deduced from the engineering constants in the usual manner. So that,

$$\boldsymbol{C} = \begin{bmatrix} 0.771 & 0.442 & 0.314 & 0 & 0 & 0 \\ 0.442 & 13.67 & 0.448 & 0 & 0 & 0 \\ 0.314 & 0.448 & 1.044 & 0 & 0 & 0 \\ 0 & 0 & 0 & 0.858 & 0 & 0 \\ 0 & 0 & 0 & 0 & 0.094 & 0 \\ 0 & 0 & 0 & 0 & 0 & 1.045 \end{bmatrix} \cdot \text{GPa} \, . \tag{49}$$

The conditions for orthotropy are listed in 1 so that it may be verified that this elasticity tensor is that of an orthotropic material by confirming

a) that it is Monoclinic: $C_{16} = C_{15} = C_{25} = C_{26} = 0,$

$C_{46} = C_{45} = C_{35} = C_{36} = 0.$

b) and that: $C_{14} = C_{24} = C_{34} = C_{56} = 0.$

The eigenvalues for this orthotropic symmetry are numerically determined as,

$$\Lambda = \begin{bmatrix} 13.68 \\ 1.219 \\ 0.564 \\ 0.858 \\ 0.094 \\ 1.045 \end{bmatrix} \cdot \text{GPa.} \tag{50}$$

The corresponding eigenvectors are

$$N1 = \begin{bmatrix} 3.499*10^{-2} \\ 0.9987 \\ 3.625*10^{-2} \\ 0 \\ 0 \\ 0 \end{bmatrix}, \quad N2 = \begin{bmatrix} 0.5398 \\ -4.942*10^{-2} \\ 0.8403 \\ 0 \\ 0 \\ 0 \end{bmatrix}, \quad N3 = \begin{bmatrix} -0.8411 \\ 9.836*10^{-3} \\ 0.5409 \\ 0 \\ 0 \\ 0 \end{bmatrix}, \quad N4 = \begin{bmatrix} 0 \\ 0 \\ 0 \\ 1 \\ 0 \\ 0 \end{bmatrix}, \quad N5 = \begin{bmatrix} 0 \\ 0 \\ 0 \\ 0 \\ 1 \\ 0 \end{bmatrix}, \quad N6 = \begin{bmatrix} 0 \\ 0 \\ 0 \\ 0 \\ 0 \\ 1 \end{bmatrix}. \tag{51}$$

The first three modal products for Douglas Fir are therefore given by

$$\begin{aligned} P^{(1)}_{\alpha\beta} T_\alpha T_\beta &= \left(3.499*10^{-2} T_1 + 0.9987 T_2 + 3.625*10^{-2} T_3\right)^2 = (\sigma^{(1)})^2, \\ P^{(2)}_{\alpha\beta} T_\alpha T_\beta &= \left(0.5398\, T_1 - 4.942*10^{-2} T_2 + 0.8403\, T_3\right)^2 = (\sigma^{(2)})^2, \\ P^{(3)}_{\alpha\beta} T_\alpha T_\beta &= \left(-0.8411\, T_1 + 9.836*10^{-3} T_2 + 0.5407\, T_3\right)^2 = (\sigma^{(3)})^2. \end{aligned} \tag{52}$$

The last three modal products reduce to maximum shear stress criteria

$$
\begin{aligned}
P^{(4)}_{\alpha\beta} T_\alpha T_\beta &= (T_4)^2 = (\sigma^{(4)})^2, \\
P^{(5)}_{\alpha\beta} T_\alpha T_\beta &= (T_5)^2 = (\sigma^{(5)})^2, \\
P^{(6)}_{\alpha\beta} T_\alpha T_\beta &= (T_6)^2 = (\sigma^{(6)})^2.
\end{aligned} \tag{53}
$$

The Wood Handbook (1974) tabulates strengths for Douglas Fir. Only uniaxial data is available for this material. Furthermore, the longitudinal tensile strength was not recorded but, as recommended by the wood handbook, the modulus of rupture is substituted here. Unfortunately no distinction between tangential and radial strengths was made in the tabulated strengths, therefore both radial and longitudinal strengths are assumed equal in this example. When converted to GPa the strengths for Douglas Fir are thus,

$$
\begin{aligned}
T_1 \text{ (tensile)} &= 2.10*10^{-3}, & T_1 \text{ (comp.)} &= 2.60*10^{-3}, \\
T_2 \text{ (tensile)} &= 53.0*10^{-3}, & T_2 \text{ (comp.)} &= 26.1*10^{-3}, \\
T_3 \text{ (tensile)} &= 2.10*10^{-3}, & T_3 \text{ (comp.)} &= 2.60*10^{-3}.
\end{aligned}
$$

Then by (29) we obtain table 2.

Table 2 List of strength data for Douglas Fir (Liu, 1984) and their corresponding Kelvin modes magnitudes in GPa.

T_1, T_2, T_3	$\sigma^{(1)}$	$\sigma^{(2)}$	$\sigma^{(3)}$
2.10E-3, 0, 0	7.349E-5	1.134E-3	-1.766E-3
-2.60E-3, 0, 0	-9.098E-5	-1.404E-3	2.187E-3
0, 53.0E-3 , 0	5.293E-2	-2.619E-3	5.213E-4
0, -26.1E-3, 0	-2.607E-2	1.290E-3	-2.567E-4
0, 0, 2.10E-3	7.613E-5	1.765E-3	1.136E-3
0, 0, -2.60E-3	-9.426E-5	-2.185E-3	-1.406E-3

The extreme values for each mode in table 2 are selected. We therefore obtain a set of six criteria for the kelvin modes:

$$\sigma^{(1)}_{max} = 5.293\text{E-}2,\ \sigma^{(1)}_{min} = -2.607\text{E-}2$$

$$\sigma^{(2)}_{max} = 1.765\text{E-}3,\ \sigma^{(2)}_{min} = -2.185\text{E-}3$$

$$\sigma^{(3)}_{max} = 2.187\text{E-}3 \text{ and } \sigma^{(3)}_{max} = -1.766\text{E-}2$$

All units are in GPa.

Then by (32) the three Kelvin modes become

Kelvin Mode 1

$$\left(\sigma^{(1)} - 5.293*10^{-2}\right)\left(\sigma^{(1)} + 2.607^{-2}\right) = 0$$
$$\text{where } \sigma^{(1)} = 3.616*10^{-2}T_1 + 0.9985T_2 + 4.1617*10^{-2}T_3 \qquad (54)$$

Kelvin Mode 2

$$\left(\sigma^{(2)} - 1.765*10^{-3}\right)\left(\sigma^{(2)} + 2.185*10^{-3}\right) = 0$$
$$\text{where } \sigma^{(2)} = 0.5023\,T_1 - 4.952*10^{-2}T_2 + 0.8633\,T_3 \qquad (55)$$

Kelvin Mode 3

$$\left(\sigma^{(3)} - 2.187 * 10^{-3}\right)\left(\sigma^{(3)} + 1.766 * 10^{-2}\right) = 0$$
$$\text{where } \sigma^{(3)} = -0.7837 T_1 + 5.555 * 10^{-3} T_2 + 0.6211 T_3 \tag{56}$$

These Kelvin modes are equations of parallel planes in the principal stress space (T_1, T_2, T_3) and, along with the maximum stress planes, represent the failure bound in this space.

The resulting modal failure envelope is illustrated in Fig. 19. The three-dimensional modal failure envelope [Fig. 19(a)] is long, narrow and oriented almost entirely along the T_2 axis. This particularity is confirmed by biaxial strength predictions of Fig. 19(b) and (c), whereas the transverse biaxial strength [Fig. 19(d)] is predictably consistent in all directions. This strong strength anisotropy in the axial direction is entirely consistent with what is known of these softwoods. Though generally uniaxial strength alone would be insufficient to completely describe the modal failure envelope, in this case the particularities of the materials may be fortuitous. Indeed, the long aspect ratio and near coincidence of the failure envelope with the T_2 axis reduces possible changes in the appearance of the failure envelope. If biaxial data were included in the evaluation of this envelope it is doubtful that it would significantly change the position of these failure surfaces. Therefore the failure envelope shown in Fig. 19 (a) through (d) may in fact, be nearly the best we can obtain with this theory.

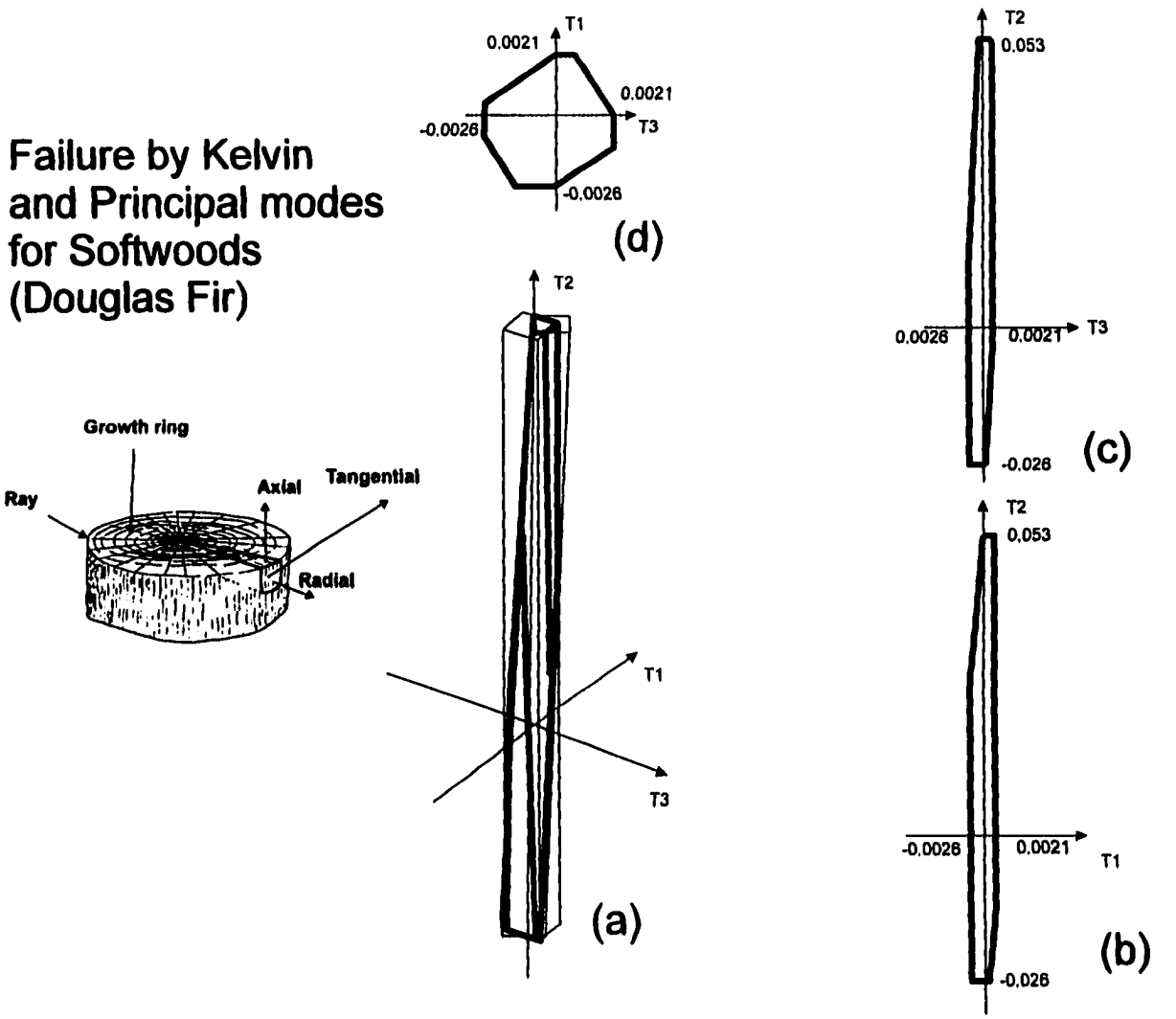

Fig. 19 (a) Plot of the failure envelope by combined Kelvin and Complementary modes in principal stress space. (b) The predicted T_1-T_2 (tangential-longitudinal) biaxial failure. (c) The predicted T_3-T_2 (radial-longitudinal) biaxial failure. (d) the predicted T_3-T_1 (radial-tangential) biaxial failure. The envelope was produced from uniaxial strength alone.

5.4.2 Numerical Example: (Softwood) Sitka Spruce

The elasticity tensor for spruce can be determined from data provided the Wood Handbook (1974):

$$C = \begin{bmatrix} 0.4425 & 0.3211 & 0.1917 & 0 & 0 & 0 \\ 0.3211 & 16.286 & 0.4422 & 0 & 0 & 0 \\ 0.1917 & 0.4422 & 0.7746 & 0 & 0 & 0 \\ 0 & 0 & 0 & 1.234 & 0 & 0 \\ 0 & 0 & 0 & 0 & 0.072 & 0 \\ 0 & 0 & 0 & 0 & 0 & 1.52 \end{bmatrix} \cdot \text{GPa}. \tag{57}$$

As in the previous example, the conditions for orthotropy are listed in 1 so that it may be verified that this elasticity tensor is indeed that of an orthotropic material. The eigenvalues for this tensor are numerically determined as

$$\Lambda = \begin{bmatrix} 16.305 \\ 0.8436 \\ 0.3542 \\ 1.234 \\ 0.0720 \\ 1.5200 \end{bmatrix} \cdot \text{GPa}, \tag{58}$$

and the corresponding eigenvectors are

$$N1 = \begin{bmatrix} 2.058*10^{-2} \\ 0.9994 \\ 2.871*10^{-2} \\ 0 \\ 0 \\ 0 \end{bmatrix}, \quad N2 = \begin{bmatrix} 0.4083 \\ -3.4611*10^{-2} \\ 0.9122 \\ 0 \\ 0 \\ 0 \end{bmatrix}, \quad N3 = \begin{bmatrix} -0.9126 \\ 7.050*10^{-3} \\ 0.4087 \\ 0 \\ 0 \\ 0 \end{bmatrix}, \quad N4 = \begin{bmatrix} 0 \\ 0 \\ 0 \\ 1 \\ 0 \\ 0 \end{bmatrix}, \quad N5 = \begin{bmatrix} 0 \\ 0 \\ 0 \\ 0 \\ 1 \\ 0 \end{bmatrix}, \quad N6 = \begin{bmatrix} 0 \\ 0 \\ 0 \\ 0 \\ 0 \\ 1 \end{bmatrix}. \tag{59}$$

The first three modal products are therefore given by

$$\begin{aligned} P^{(1)}_{\alpha\beta}T_\alpha T_\beta &= \left(2.058*10^{-2}T_1+0.9994T_2+2.871*10^{-2}T_3\right)^2 = (\sigma^{(1)})^2, \\ P^{(2)}_{\alpha\beta}T_\alpha T_\beta &= \left(0.4083T_1-3.461*10^{-2}T_2+0.9122T_3\right)^2 = (\sigma^{(2)})^2. \\ P^{(3)}_{\alpha\beta}T_\alpha T_\beta &= \left(-0.9126T_1+7.050*10^{-3}T_2+0.4087T_3\right)^2 = (\sigma^{(3)})^2. \end{aligned} \tag{60}$$

The last three modal products reduce to maximum shear stress criteria

$$\begin{aligned} P^{(4)}_{\alpha\beta}T_\alpha T_\beta &= (T_4)^2 = (\sigma^{(4)})^2, \\ P^{(5)}_{\alpha\beta}T_\alpha T_\beta &= (T_5)^2 = (\sigma^{(5)})^2, \\ P^{(6)}_{\alpha\beta}T_\alpha T_\beta &= (T_6)^2 = (\sigma^{(6)})^2. \end{aligned} \tag{61}$$

Only uniaxial strength data is available for this material. Liu (1984) list reasonable strength values for Sitka Spruce which, when converted to GPa are

T_1 (tensile) = $2.55*10^{-3}$ T_1 (comp.) = $4.0*10^{-3}$

T_2 (tensile) = $79.3*10^{-3}$ T_2 (comp.) = $38.7*10^{-3}$

T_3 (tensile) = $2.55*10^{-3}$ T_3 (comp.) = $4.0*10^{-3}$

Then by (29) we obtain table 3.

Table 3 List of strength data for Sitka Spruce (Liu, 1984) and their corresponding Kelvin modes magnitudes in GPa.

T_1, T_2, T_3	$\sigma^{(1)}$	$\sigma^{(2)}$	$\sigma^{(3)}$
2.55E-3, 0, 0	5.249E-5	1.042E-3	-2.328E-3
-4.0E-3, 0, 0	-8.229E-5	-1.633E-3	3.649E-3
0, 79.3E-3 , 0	7.924E-2	-2.744E-3	5.590E-4
0, -38.7E-3, 0	-3.866E-2	1.339E-3	-2.727E-4
0, 0, 2.55E-3	7.324E-5	2.327E-3	1.043E-3
0, 0, -4.0E-3	-1.148E-4	-3.648E-3	-1.634E-3

The extreme values for each mode in table 3 are selected. We therefore get a set of six criteria for the Kelvin modes:

$$\sigma^{(1)}_{max} = 7.924\text{E-}2,\ \sigma^{(1)}_{min} = -3.866\text{E-}2,$$

$$\sigma^{(2)}_{max} = 2.327\text{E-}3,\ \sigma^{(2)}_{min} = -3.648\text{E-}3,$$

$$\sigma^{(3)}_{max} = 3.649\text{E-}3 \text{ and } \sigma^{(3)}_{max} = -2.328\text{E-}2.$$

All units are in GPa.

Then by (32) the three Kelvin modes become

Kelvin Mode 1

$$\begin{aligned} &\left(\sigma^{(1)} - 7.924*10^{-2}\right)\left(\sigma^{(1)} + 3.866*10^{-2}\right) = 0 \\ &\text{where } \sigma^{(1)} = \left(2.058*10^{-2}T_1 + 0.9994T_2 + 2.871*10^{-2}T_3\right) \end{aligned} \tag{62}$$

Kelvin Mode 2

$$\begin{aligned} &\left(\sigma^{(2)} - 2.327*10^{-3}\right)\left(\sigma^{(2)} + 3.648*10^{-3}\right) = 0 \\ &\text{where } \sigma^{(2)} = 0.4083T_1 - 3.461*10^{-2}T_2 + 0.9122T_3 \end{aligned} \tag{63}$$

Kelvin Mode 3

$$\begin{aligned} &\left(\sigma^{(3)} - 3.650*10^{-3}\right)\left(\sigma^{(3)} + 2.328*10^{-2}\right) = 0 \\ &\text{where } \sigma^{(3)} = -0.9126T_1 + 7.050*10^{-3}T_2 + 0.4087T_3 \end{aligned} \tag{64}$$

These Kelvin modes are equations of parallel planes in the principal stress space (T_1, T_2, T_3), and along with the maximum stress planes, represent the failure bound in this space.

The resulting failure three-dimensional envelope for Sitka spruce is plotted in Fig. 20(a) and the corresponding biaxial traces in Fig. 20(b), (c) and (d). Like the previous softwood example, the failure envelope is that of a highly anisotropic material. The envelope

is long and narrow and oriented almost entirely in the T_2 (axial) direction. Because of this feature it is likely that this envelope, would also not have greatly benefited from multiaxial strength. Both the Kelvin and principal modes are nearly coincident, making this envelope almost completely defined.

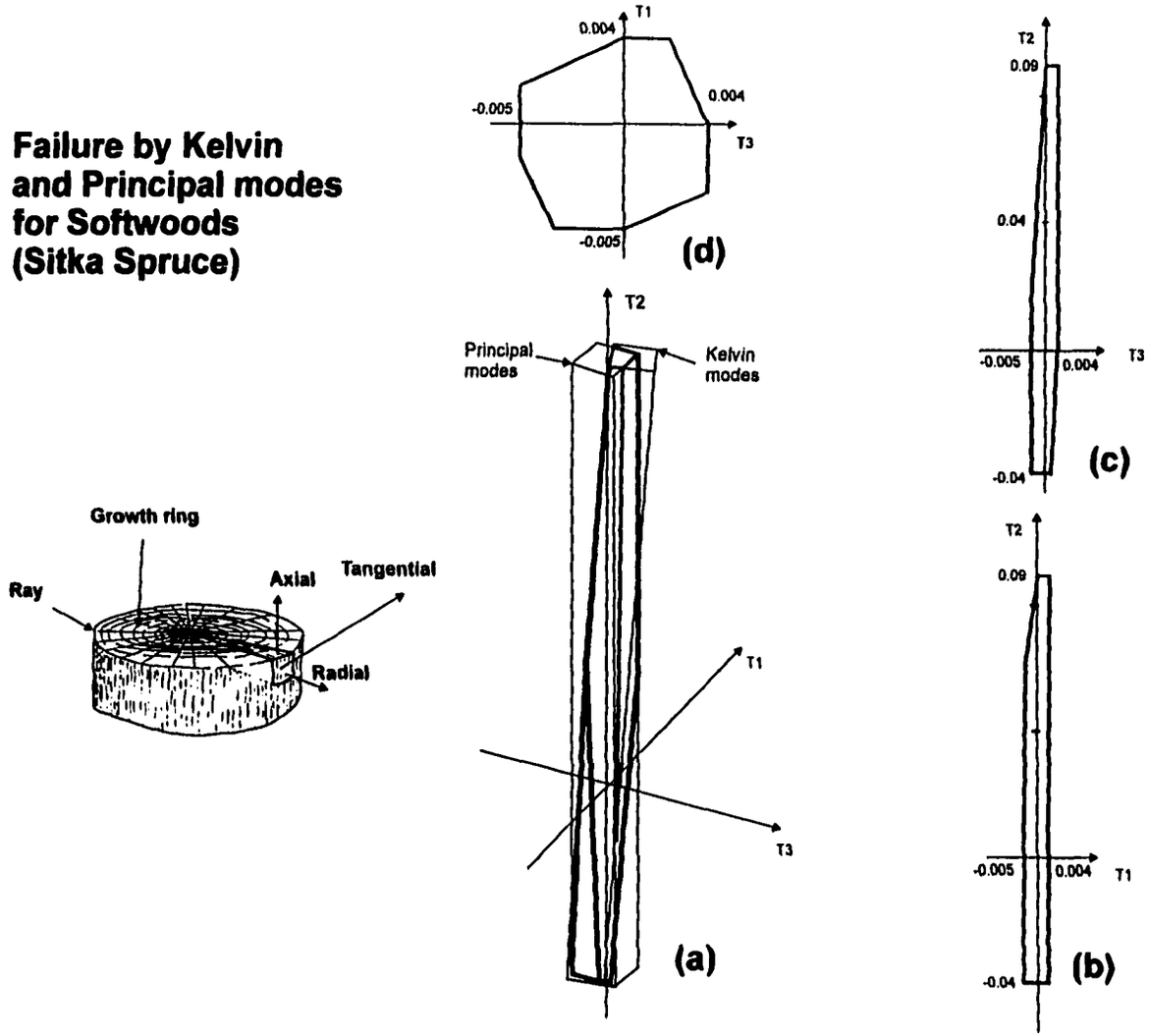

Fig. 20 (a) Plot of the failure envelope for Sitka spruce by combined Kelvin and Complementary modes in principal stress space. (b) The predicted T_1-T_2 (tangential-longitudinal) biaxial failure. (c) The predicted T_3-T_2 (radial-longitudinal) biaxial failure. (d) the predicted T_3-T_1 (radial-tangential) biaxial failure. The envelope was produced from uniaxial strength alone.

5.4.3 Numerical example: (Hardwood) Yellow Birch

The engineering constants for yellow birch are tabulated in the Wood Handbook (1974). They are,

$E_1 = 0.695$ GPa $\quad E_2 = 13.9$ GPa $\quad E_3 = 1.084$ GPa

$\nu_{13} = 0.447$ $\quad \nu_{23} = 0.426$ $\quad \nu_{12} = 0.023$

$\nu_{31} = 0.697$ $\quad \nu_{32} = 0.033$ $\quad \nu_{21} = 0.451(+0.001)$

$G_{23} = 2.364$ GPa $\quad G_{13} = 1.029$ GPa $\quad G_{12} = 0.945$ GPa

where indices 1, 2, 3 represent the tangential, longitudinal and radial direction, respectively, and where the values in parentheses are adjustments made to accommodate the symmetry of the compliance and elasticity tensor. Furthermore it should be noted that the values for ν_{13} and ν_{32} appear to have been substituted for each other in the reference (Wood Handbook, 1974). They are corrected here and the resulting elasticity tensor is then

$$\boldsymbol{C} = \begin{bmatrix} 1.053 & 0.799 & 0.76 & 0 & 0 & 0 \\ 0.799 & 14.69 & 1.035 & 0 & 0 & 0 \\ 0.76 & 1.035 & 1.649 & 0 & 0 & 0 \\ 0 & 0 & 0 & 1.029 & 0 & 0 \\ 0 & 0 & 0 & 0 & 2.364 & 0 \\ 0 & 0 & 0 & 0 & 0 & 0.945 \end{bmatrix} \cdot \text{GPa}. \tag{65}$$

The conditions for orthotropy are listed in 1 so that it may be verified that this elasticity tensor is indeed that of an orthotropic material. The eigenvalues for this orthotropic symmetry are numerically determined as

$$\Lambda = \begin{bmatrix} 14.82 \\ 2.033 \\ 0.534 \\ 1.029 \\ 2.364 \\ 0.945 \end{bmatrix} \cdot \text{GPa.} \tag{66}$$

The corresponding eigenvectors are

$$N1 = \begin{bmatrix} 6.227E-2 \\ 0.9947 \\ 8.178E-2 \\ 0 \\ 0 \\ 0 \end{bmatrix}, \quad N2 = \begin{bmatrix} 0.5563 \\ -0.1026 \\ 0.8246 \\ 0 \\ 0 \\ 0 \end{bmatrix}, \quad N3 = \begin{bmatrix} -0.8286 \\ 5.858E-3 \\ 0.5597 \\ 0 \\ 0 \\ 0 \end{bmatrix}, \quad N4 = \begin{bmatrix} 0 \\ 0 \\ 0 \\ 1 \\ 0 \\ 0 \end{bmatrix}, \quad N5 = \begin{bmatrix} 0 \\ 0 \\ 0 \\ 0 \\ 1 \\ 0 \end{bmatrix}, \quad N6 = \begin{bmatrix} 0 \\ 0 \\ 0 \\ 0 \\ 0 \\ 1 \end{bmatrix} \tag{67}$$

The first three modal products for Birch are therefore given by

$$\begin{aligned} P^{(1)}_{\alpha\beta} T_\alpha T_\beta &= \left(6.227 * 10^{-2} T_1 + 0.9947 T_2 + 8.178 * 10^{-2} T_3\right)^2 = (\sigma^{(1)})^2. \\ P^{(2)}_{\alpha\beta} T_\alpha T_\beta &= \left(0.5563 T_1 - 0.1026 T_2 + 0.8246 T_3\right)^2 = (\sigma^{(2)})^2. \\ P^{(3)}_{\alpha\beta} T_\alpha T_\beta &= \left(-0.8286 T_1 + 5.858 * 10^{-3} T_2 + 0.5597 T_3\right)^2 = (\sigma^{(3)})^2. \end{aligned} \tag{68}$$

The last three modal products reduce to maximum shear stress criteria

$$\begin{aligned} P^{(4)}_{\alpha\beta} T_\alpha T_\beta &= (T_{23})^2 = (\sigma^{(4)})^2, \\ P^{(5)}_{\alpha\beta} T_\alpha T_\beta &= (T_{13})^2 = (\sigma^{(5)})^2, \\ P^{(6)}_{\alpha\beta} T_\alpha T_\beta &= (T_{12})^2 = (\sigma^{(6)})^2. \end{aligned} \tag{69}$$

The Wood Handbook (1974) tabulates strengths for yellow Birch. Only uniaxial data is available for this material. Furthermore, the longitudinal tensile strength was not recorded but, as recommended by the Wood Handbook (1974), the modulus of rupture is substituted here. Unfortunately no distinction between tangential and radial strengths was made in the

tabulated strengths, therefore both radial and longitudinal strengths are assumed equal in this example. When converted to GPa the tabulated strengths for yellow birch are therefore,

$$T_1 \text{ (tensile)} = 5.50*10^{-3}, \qquad T_1 \text{ (comp.)} = 7.10*10^{-3},$$

$$T_2 \text{ (tensile)} = 99.0*10^{-3}, \qquad T_2 \text{ (comp.)} = 46.6*10^{-3},$$

$$T_3 \text{ (tensile)} = 5.50*10^{-3}, \qquad T_3 \text{ (comp.)} = 7.10*10^{-3}.$$

Then by (29) we obtain table 4.

Table 4 List of strength data for yellow Birch and their corresponding Kelvin modes magnitudes in GPa.

T_1, T_2, T_3	$\sigma^{(1)}$	$\sigma^{(2)}$	$\sigma^{(3)}$
5.50E-3, 0, 0	3.425E-4	3.060E-3	-4.557E-3
-7.10E-3, 0, 0	-4.359E-4	-3.894E-3	5.800E-3
0, 99.0E-3, 0	9.848E-2	-1.016E-2	5.799E-4
0, -46.6E-3, 0	-4.635E-2	4.781E-3	-2.73E-4
0, 0, 5.50E-3	4.498E-4	4.535E-3	3.078E-3
0, 0, -7.10E-3	-5.724E-4	-5.772E-3	-3.918E-3

The extreme values for each mode in table 4 are selected. We therefore get a set of six criteria for the Kelvin modes:

$$\sigma^{(1)}_{max} = 9.848\text{E-}2, \ \sigma^{(1)}_{min} = -4.635\text{E-}2$$

$$\sigma^{(2)}_{max} = 4.781\text{E-}3, \ \sigma^{(2)}_{min} = -1.016\text{E-}2$$

$$\sigma^{(3)}_{max} = 5.800\text{E-}3 \text{ and } \sigma^{(3)}_{max} = -4.557\text{E-}2$$

All units are in GPa.

Then by (32) the three Kelvin modes become

Mode 1

$$\begin{aligned} &\left(\sigma^{(1)} - 5.292 * 10^{-2}\right)\left(\sigma^{(1)} + -2.606^{-2}\right) = 0 \\ &\text{where } \sigma^{(1)} = 3.616 * 10^{-2} T_1 + 0.9985 T_2 + 4.1617 * 10^{-2} T_3 \end{aligned} \tag{70}$$

Mode 2

$$\begin{aligned} &\left(\sigma^{(2)} - 1.813 * 10^{-3}\right)\left(\sigma^{(2)} + 2.625 * 10^{-2}\right) = 0 \\ &\text{where } \sigma^{(2)} = 0.5023 T_{11} - 4.952 * 10^{-2} T_{22} + 0.8633 T_{33} \end{aligned} \tag{71}$$

Mode 3

$$\begin{aligned} &\left(\sigma^{(3)} - 2.038 * 10^{-3}\right)\left(\sigma^{(3)} + 2.606 * 10^{-2}\right) = 0 \\ &\text{where } \sigma^{(3)} = -0.7837 T_1 + 5.555 * 10^{-3} T_2 + 0.6211 T_3 \end{aligned} \tag{72}$$

The resulting failure three-dimensional envelope for yellow birch is plotted in Fig. 21(a) and the corresponding biaxial traces in Fig. 21(b), (c) and (d). Like the softwoods, this wood displays a similarly long and narrow failure envelope oriented almost entirely in the T_2 (axial) direction. This envelope however is slightly wider and not as long as the softwoods. This is entirely consistent with what is known of the difference between hard and softwood strength. Nevertheless, like the previous examples, this modal failure envelope is very nearly defined and would not have greatly benefited from multiaxial strength.

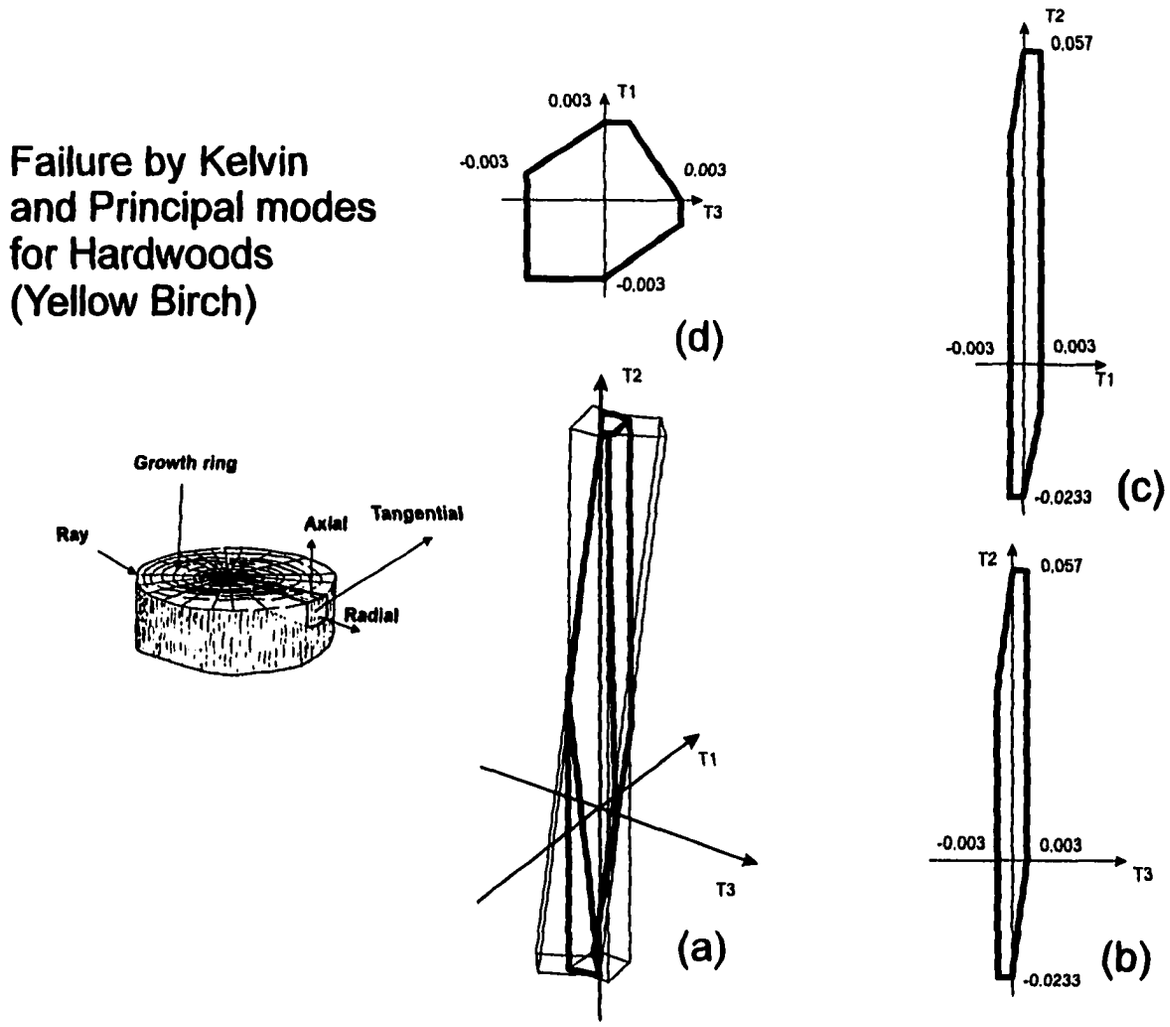

Fig. 21 (a) Plot of the failure envelope by combined Kelvin and Complementary modes in principal stress space of a hardwood (yellow birch). (b) The predicted T_1-T_2 (tangential-longitudinal) biaxial failure. (c) The predicted T_3-T_2 (radial-longitudinal) biaxial failure. (d) the predicted T_3-T_1 (radial-tangential) biaxial failure. The envelope was produced from uniaxial strength alone.

5.4.4 Numerical example: (Hardwood) Northern Red Oak

The elasticity tensor for an Oak specimen was measured by François (1995) as

$$\boldsymbol{C} = \begin{bmatrix} 2.62 & 0.88 & 0.99 & 0 & 0 & 0 \\ 0.88 & 13.2 & 0.61 & 0 & 0 & 0 \\ 0.99 & 0.61 & 4.44 & 0 & 0 & 0 \\ 0 & 0 & 0 & 1.32 & 0 & 0 \\ 0 & 0 & 0 & 0 & 1.6 & 0 \\ 0 & 0 & 0 & 0 & 0 & 1.04 \end{bmatrix} \cdot \text{GPa} \, . \tag{73}$$

As in the previous examples, the conditions for orthotropy are listed in 1 so that it may be verified that this elasticity tensor is that of an orthotropic material. The eigenvalues for this orthotropic symmetry are numerically determined as,

$$\Lambda = \begin{bmatrix} 13.327 \\ 4.777 \\ 2.156 \\ 1.32 \\ 1.6 \\ 1.04 \end{bmatrix} \cdot \text{GPa} \, , \tag{74}$$

The corresponding eigenvectors are

$$N1 = \begin{bmatrix} 8.883E-2 \\ 0.9930 \\ 7.806E-2 \\ 0 \\ 0 \\ 0 \end{bmatrix}, \; N2 = \begin{bmatrix} 0.3786 \\ -0.1061 \\ 0.9194 \\ 0 \\ 0 \\ 0 \end{bmatrix}, \; N3 = \begin{bmatrix} -0.9213 \\ 5.212E-2 \\ 0.3854 \\ 0 \\ 0 \\ 0 \end{bmatrix}, \; N4 = \begin{bmatrix} 0 \\ 0 \\ 0 \\ 1 \\ 0 \\ 0 \end{bmatrix}, \; N5 = \begin{bmatrix} 0 \\ 0 \\ 0 \\ 0 \\ 1 \\ 0 \end{bmatrix}, \; N6 = \begin{bmatrix} 0 \\ 0 \\ 0 \\ 0 \\ 0 \\ 1 \end{bmatrix} \tag{75}$$

The first three modal products for oak are therefore given by

$$
\begin{aligned}
P^{(1)}_{\alpha\beta}T_\alpha T_\beta &= \left(8.883*10^{-2}T_1+0.9930T_2+7.806*10^{-2}T_3\right)^2 = (\sigma^{(1)})^2.\\
P^{(2)}_{\alpha\beta}T_\alpha T_\beta &= \left(0.3786T_1-0.1061T_2+0.9194T_3\right)^2 = (\sigma^{(2)})^2.\\
P^{(3)}_{\alpha\beta}T_\alpha T_\beta &= \left(-0.9213T_1+5.212*10^{-2}T_2+0.3854T_3\right)^2 = (\sigma^{(3)})^2.
\end{aligned}
\tag{76}
$$

The last three modal products reduce to maximum shear stress criteria

$$
\begin{aligned}
P^{(4)}_{\alpha\beta}T_\alpha T_\beta &= (T_4)^2 = (\sigma^{(4)})^2,\\
P^{(5)}_{\alpha\beta}T_\alpha T_\beta &= (T_5)^2 = (\sigma^{(5)})^2,\\
P^{(6)}_{\alpha\beta}T_\alpha T_\beta &= (T_6)^2 = (\sigma^{(6)})^2.
\end{aligned}
\tag{77}
$$

The Wood Handbook (1974) lists reasonable strengths for different oak varieties. The values for northern red oak are selected here because the reported longitudinal modulus is close to that of François (1995). Only uniaxial data is available for this material. Furthermore, the longitudinal tensile strength was not recorded but, as recommended by the Wood Handbook (1974), the modulus of rupture is substituted here. Unfortunately no distinction between tangential and radial strengths was made in the tabulated strengths; therefore, both radial and longitudinal strengths are assumed equal in this example. When converted to GPa the tabulated strengths for northern red oak are therefore

$$
\begin{aligned}
T_1 \text{ (tensile)} &= 5.50*10^{-3}, \qquad T_1 \text{ (comp.)} = 7.00*10^{-3},\\
T_2 \text{ (tensile)} &= 99.0*10^{-3}, \qquad T_2 \text{ (comp.)} = 46.6*10^{-3},\\
T_3 \text{ (tensile)} &= 5.50*10^{-3}, \qquad T_3 \text{ (comp.)} = 7.00*10^{-3}.
\end{aligned}
$$

Then by (29) we obtain the mode magnitudes and list them in table 5.

Table 5 List of strength data for northern red oak and their corresponding Kelvin modes magnitudes in GPa.

T_1, T_2, T_3	$\sigma^{(1)}$	$\sigma^{(2)}$	$\sigma^{(3)}$
5.50E-3, 0, 0	4.886E-4	2.083E-3	-5.067E-3
-7.00E-3, 0, 0	-6.218E-4	-2.650E-3	6.449E-3
0, 99.0E-3, 0	9.831E-2	-1.051E-2	5.160E-3
0, -46.6E-3, 0	-4.627E-2	4.947E-3	-2.429E-3
0, 0, 5.50E-3	4.293E-4	5.057E-3	2.120E-3
0, 0, -7.00E-3	-5.464E-4	-6.436E-3	-2.698E-3

The extreme values of each mode in table 5 are selected. We therefore get a set of six criteria for the Kelvin modes:

$$\sigma^{(1)}_{max} = 9.831\text{E-}2,\ \sigma^{(1)}_{min} = -4.627\text{E-}2,$$

$$\sigma^{(2)}_{max} = 5.057\text{E-}3,\ \sigma^{(2)}_{min} = -1.051\text{E-}2,$$

$$\sigma^{(3)}_{max} = 6.449\text{E-}3 \text{ and } \sigma^{(3)}_{max} = -5.067\text{E-}3.$$

All units are in GPa.

Then by (32) the three Kelvin modes become

Kelvin Mode 1

$$\left(\sigma^{(1)} - 9.831*10^{-2}\right)\left(\sigma^{(1)} + 4.627*10^{-2}\right) = 0$$
$$\text{where } \sigma^{(1)} = 8.8833*10^{-2}T_1 + 0.9930T_2 + 7.8057*10^{-2}T_3 \qquad (78)$$

Kelvin Mode 2

$$\left(\sigma^{(2)} - 5.057 * 10^{-3}\right)\left(\sigma^{(2)} + 1.051 * 10^{-2}\right) = 0$$
$$\text{where } \sigma^{(2)} = 0.3786 T_1 - 0.1061 T_2 + 0.9194 T_3 \tag{79}$$

Kelvin Mode 3

$$\left(\sigma^{(3)} - 6.449 * 10^{-3}\right)\left(\sigma^{(3)} + 5.067 * 10^{-3}\right) = 0$$
$$\text{where } \sigma^{(3)} = -0.9213 T_1 + 5.212 * 10^{-2} T_2 + 0.3854 T_3 \tag{80}$$

The resulting three-dimensional modal failure envelope for northern red oak is illustrated in Fig. 22(a) and its corresponding biaxial traces in Fig. 22(b), (c) and (d). This hardwood displays the same characteristics exhibited by yellow birch: a long and narrow failure envelope oriented almost entirely in the T_2 (axial) direction. This modal failure envelope is slightly wider and not as long as the softwoods. This is, again, entirely consistent with what is known of the difference between hard and softwood strength. Nevertheless, like the previous examples this modal failure envelope is very nearly defined and would not have greatly benefited from multiaxial strength.

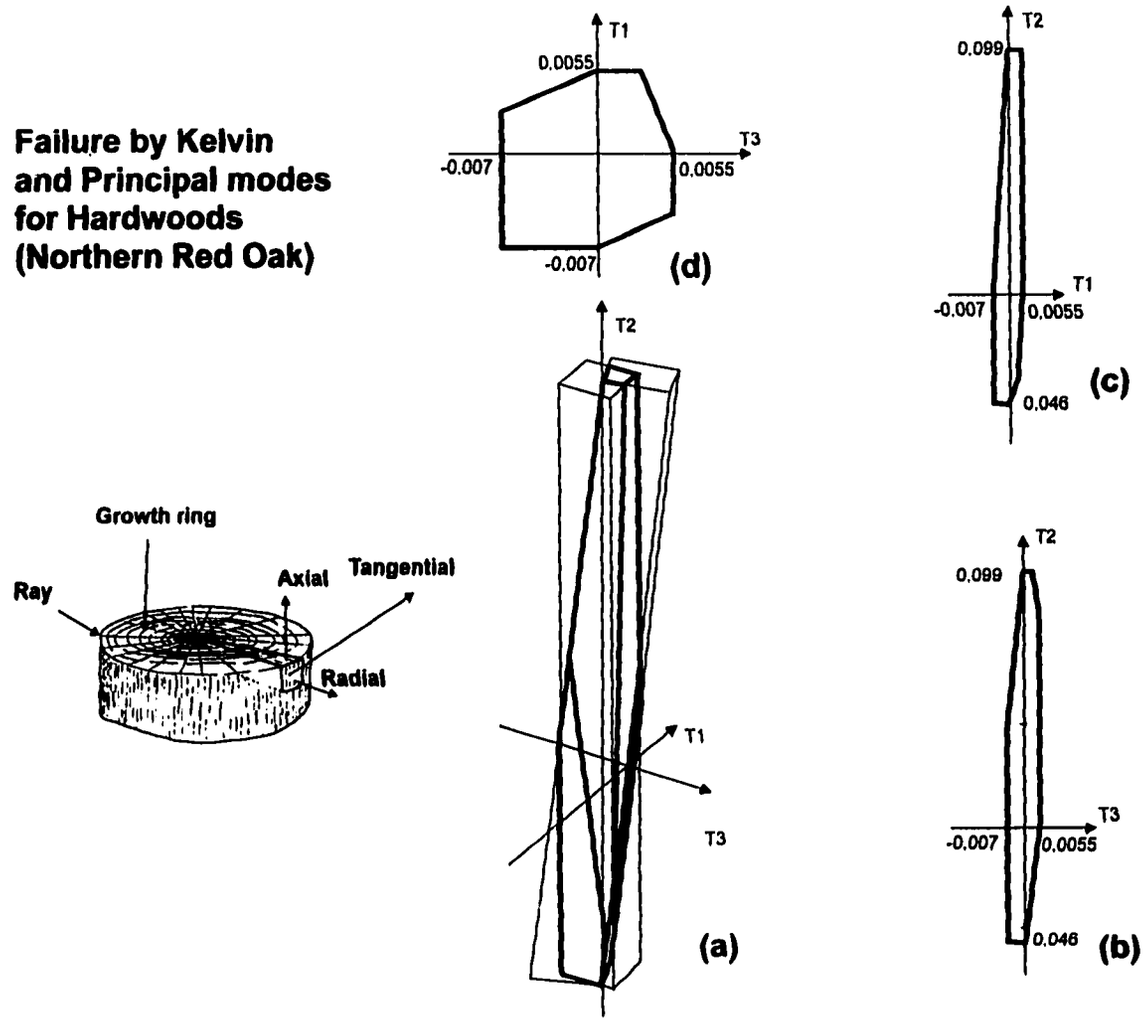

Fig. 22 (a) Plot of the failure envelope by combined Kelvin and Complementary modes in principal stress space of a hardwood (northern red oak). (b) The predicted T_1-T_2 (tangential-longitudinal) biaxial failure. (c) The predicted T_3-T_2 (radial-longitudinal) biaxial failure. (d) the predicted T_3-T_1 (radial-tangential) biaxial failure. The envelope was produced from uniaxial strength alone.

5.5 Numerical example: Bovine Cortical Bone (Orthotropic)

Much of the mechanical data for bovine cortical bone is reported in Cowin (1989). The symmetry of cortical bone is generally considered to be orthotropic. Cowin (1979) reports the engineering constants for bovine cortical bone (originally reported by Van Buskirk *et al.*, 1981) as

$E_1 = 11.6$ GPa $\quad E_2 = 14.6$ GPa $\quad E_3 = 21.9$ GPa

$\nu_{13} = 0.109$ $\quad \nu_{23} = 0.205$ $\quad \nu_{12} = 0.302$

$\nu_{31} = 0.206$ $\quad \nu_{32} = 0.307$ $\quad \nu_{21} = 0.380$

$G_{13} = 6.29$ GPa $\quad G_{23} = 6.99$ GPa $\quad G_{12} = 5.29$ GPa

The elasticity tensor is obtained in the usual manner as,

$$\boldsymbol{C} = \begin{bmatrix} 14.04 & 6.33 & 4.83 & 0 & 0 & 0 \\ 6.33 & 18.4 & 6.97 & 0 & 0 & 0 \\ 4.83 & 6.97 & 25.04 & 0 & 0 & 0 \\ 0 & 0 & 0 & 6.99 & 0 & 0 \\ 0 & 0 & 0 & 0 & 6.29 & 0 \\ 0 & 0 & 0 & 0 & 0 & 5.29 \end{bmatrix} \cdot \text{GPa}. \tag{81}$$

The conditions for orthotropy are listed in table 1 so that it may be verified that this elasticity tensor is that of an orthotropic material. The eigenvalues for this orthotropic symmetry are numerically determined as

$$\Lambda = \begin{bmatrix} 32.5 \\ 15.4 \\ 9.54 \\ 6.99 \\ 6.29 \\ 5.29 \end{bmatrix} \cdot \text{GPa} \ . \tag{82}$$

The corresponding eigenvectors are

$$N1 = \begin{bmatrix} 0.381 \\ 0.541 \\ 0.75 \\ 0 \\ 0 \\ 0 \end{bmatrix}, \ N2 = \begin{bmatrix} -0.443 \\ -0.604 \\ 0.662 \\ 0 \\ 0 \\ 0 \end{bmatrix}, \ N3 = \begin{bmatrix} 0.811 \\ -0.585 \\ 9.92E\text{-}3 \\ 0 \\ 0 \\ 0 \end{bmatrix}, \ N4 = \begin{bmatrix} 0 \\ 0 \\ 0 \\ 1 \\ 0 \\ 0 \end{bmatrix}, \ N5 = \begin{bmatrix} 0 \\ 0 \\ 0 \\ 0 \\ 1 \\ 0 \end{bmatrix}, \ N6 = \begin{bmatrix} 0 \\ 0 \\ 0 \\ 0 \\ 0 \\ 1 \end{bmatrix}. \tag{83}$$

The first three modal products for cortical bone are therefore given by

$$\begin{aligned} P^{(1)}_{\alpha\beta} T_\alpha T_\beta &= \left(0.381 T_1 + 0.541 T_2 + 0.75 T_3\right)^2 = (\sigma^{(1)})^2, \\ P^{(2)}_{\alpha\beta} T_\alpha T_\beta &= \left(-0.444 T_1 - 0.604 T_2 + 0.662 T_3\right)^2 = (\sigma^{(2)})^2, \\ P^{(3)}_{\alpha\beta} T_\alpha T_\beta &= \left(0.811 T_1 - 0.585 T_2 + 9.92 * 10^{-2} T_3\right)^2 = (\sigma^{(3)})^2. \end{aligned} \tag{84}$$

The last three modal products reduce to maximum shear stress criteria

$$\begin{aligned} P^{(4)}_{\alpha\beta} T_\alpha T_\beta &= (T_{23})^2 = (\sigma^{(4)})^2, \\ P^{(5)}_{\alpha\beta} T_\alpha T_\beta &= (T_{13})^2 = (\sigma^{(5)})^2, \\ P^{(6)}_{\alpha\beta} T_\alpha T_\beta &= (T_{12})^2 = (\sigma^{(6)})^2. \end{aligned} \tag{85}$$

Though much of the cortical bone strength data provided by Cowin (1989) are uniaxial, the constants for an orthotropic Tsai-Wu criterion were provided for bovine cortical bone (eq.(9)). As mentioned earlier eq.(9) exhibits no bound for triaxial compressive strength. Therefore, a comparison of the modal and Tsai-Wu triaxial failure envelope would

serve no purpose other than to indicate that the modal theory is the only one of the two which does provide a triaxial compression bound. Nevertheless, the biaxial failure prediction of Tsai-Wu criterion (9) may be compared to those of the modal failure [(84) and (85)]. Using the uniaxial strength data, the bounds for the Kelvin and complementary modes are obtained and tabulated in table 6.

Table 6 List of failure data for bovine cortical bone (Cowin, 1989) and their corresponding Kelvin modes magnitudes in GPa.

T_1, T_2, T_3	$\sigma^{(1)}$	$\sigma^{(2)}$	$\sigma^{(3)}$
.039, 0, 0	0.0149	-0.0173	0.0316
-.190, 0, 0	-0.0724	0.0843	-0.154
0, .050, 0	0.0271	-0.0302	-0.0292
0, -.150, 0	-0.0812	0.0906	0.0877
0, 0, .156	0.117	0.103	0.00155
0, 0, -.237	-0.178	-0.157	-0.00235

The extreme values for each mode in table 6 are selected. We therefore obtain a set of six bounds for the Kelvin modes:

$$\sigma^{(1)}_{max} = 0.117,\ \sigma^{(1)}_{min} = -0.178$$

$$\sigma^{(2)}_{max} = 0.103,\ \sigma^{(2)}_{min} = -0.157$$

$$\sigma^{(3)}_{max} = 0.0877 \text{ and } \sigma^{(3)}_{min} = -0.154$$

All units are in GPa.

Then by (32) the three Kelvin modes become

Kelvin Mode 1

$$\left(\sigma_K^{(1)} - 0.117\right)\left(\sigma_K^{(1)} + 0.178\right) = 0$$
$$\text{where } \sigma_K^{(1)} = 0.381T_1 + 0.541T_2 + 0.75T_3 \tag{86}$$

Kelvin Mode 2

$$\left(\sigma^{(2)} - 0.103\right)\left(\sigma^{(2)} + 0.157\right) = 0$$
$$\text{where } \sigma^{(2)} = -0.444T_1 - 0.604T_2 + 0.662T_3 \tag{87}$$

Kelvin Mode 3

$$\left(\sigma^{(3)} - 0.0877\right)\left(\sigma^{(3)} + 0.157\right) = 0$$
$$\text{where } \sigma^{(3)} = 0.811T_1 - 0.585T_2 + 9.92 * 10^{-2}T_3 \tag{88}$$

These Kelvin modes are equations of parallel planes in the principal stress space (T_{11}, T_{22}, T_{33}). The three complementary principal stress modes are simply the uniaxial data.

P Mode 1

$$\left(\sigma_P^{(1)} - 45.72\right)\left(\sigma_P^{(1)} + 520.1\right) = 0,$$
$$\text{where } \sigma_P^{(1)} = T_{11}, \tag{89}$$

P Mode 2

$$\left(\sigma_P^{(2)} - 65.01\right)\left(\sigma_P^{(2)} + 215.9\right) = 0$$
$$\text{where } \sigma_P^{(2)} = T_{22} \tag{90}$$

P Mode 3

$$\left(\sigma_P^{(3)} - 146.7\right)\left(\sigma^{(3)} + 1601\right) = 0$$
$$\text{where } \sigma_P^{(3)} = T_{33} \tag{91}$$

These six modes represent the failure bound in this stress space.

The resulting modal failure envelope is plotted in principal stress space [Fig. 23(a)]. The biaxial traces of the bovine Tsai-Wu criterion suggested by Cowin (1989) are

superimposed on the corresponding planes. Of the two criteria, only the modal theory provides a closed envelope. The biaxial intercepts of the modal surface are also plotted over the corresponding Tsai-Wu envelope [Fig. 23(b), (c) and (d)]. Clearly both theories predict very different biaxial strengths. Though the modal envelope would have greatly benefited from the inclusion of biaxial strength in its formulation, it is unclear that it would have agreed with the Tsai-Wu in any case. The orientations of the Kelvin modes indicate that, had some biaxial data been included, the modal failure envelope would have been oriented in a very different direction than that of the Tsai-Wu. One possible reason for the disagreement is the reliance of the Tsai-Wu of Cowin (1989) on the in-plane shear strengths rather than on the elastic tensor as the modal surface does. Indeed, the Tsai-Wu of Cowin (1989) does not represent a fit of biaxial strength data but is rather an estimate of the biaxial strength from measured shear strengths. The value of either theories depends on how well each of them agrees with genuinely biaxial strength data. Until this data is available any further comparison is difficult.

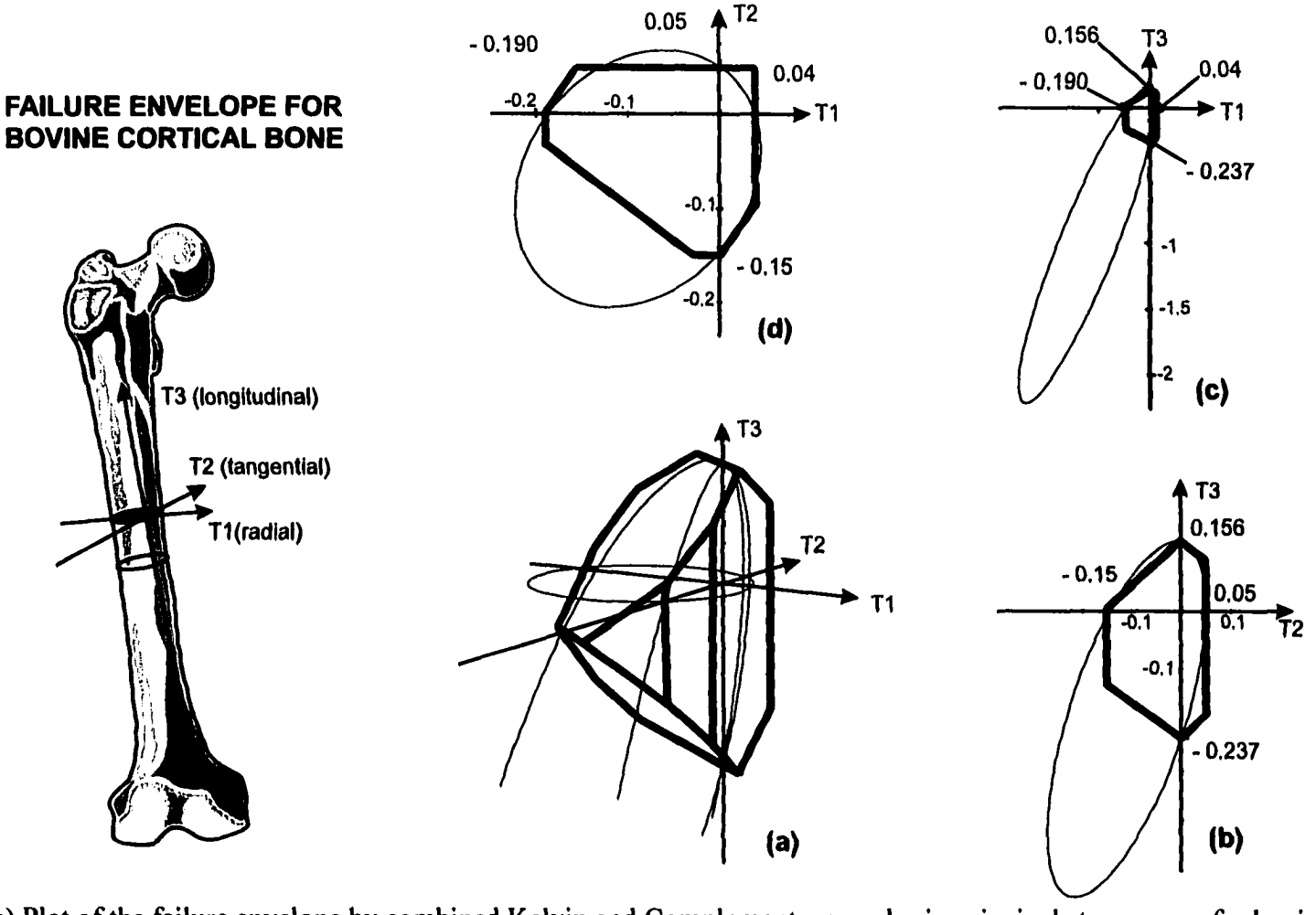

Fig. 23 (a) Plot of the failure envelope by combined Kelvin and Complementary modes in principal stress space for bovine cortical bone. The two-dimensional prediction of the bovine Tsai-Wu criterion (Cowin, 1989) are superimposed on the corresponding planes. (b) The predicted T1-T2 (tangential-longitudinal) biaxial failure superimposed over the corresponding Tsai-Wu. The predicted T3-T2 (radial-longitudinal) and Tsai-Wu biaxial failure. (d) the predicted T3-T1 (radial-tangential) and Tsai-Wu biaxial failure. The modal failure envelope was produced from uniaxial strength alone.

6 DISCUSSION

In general, the modal failure envelopes require the determination of the complete elasticity tensor along with a set of multiaxial failure data for the same material specimen. The elasticity tensor, or more specifically, its eigenvectors, are necessary to establish both the symmetry and then the orientation of the Kelvin mode failure surfaces. Though the elastic tensor is available for some materials, after an exhaustive search in the past literature no triaxial strength data was found for any anisotropic material. Thus a more complete validation of this theory must be postponed until such data is available.

It is possible that biaxial strength in three orthogonal planes may be sufficient to provide a close estimate of the modal failure envelope. The paperboard example benefited greatly from the inclusion of two sets of such data. However, as in the paperboard example, no transverse biaxial strength data was found in the literature for any anisotropic material. Most often when biaxial data is available, it is for a single plane of symmetry. For transversely isotropic materials such as unidirectional fiber reinforced laminae and tetragonal materials such as paperboard, it is reasonable to assume that the biaxial strength distributions are identical in both longitudinal planes. However, the transverse biaxial strength of a unidirectional fiber reinforced material is understandably of little interest to engineers. So it should come as no surprise that this data could not be found. Furthermore, the published biaxial strength data is often estimated from off-axis coupon testing rather than an actual biaxial test. Implicit in such cases is the assumption that the biaxial strength is a function of the in-plane shear strength. The bovine cortical bone Tsai-Wu of Cowin (1989), for instance, was developed from such an assumption. Though this may be true for some cases, including

paperboard, it has not been established as a general rule. For the modal theory it is the material's elasticity tensor, or more specifically its principal directions which governs the orientation of the Kelvin modes and therefore of the modal failure envelope. The aspect ratio of the modal envelope is affected by the magnitudes of the multiaxial strengths. Therefore it is necessary that genuinely biaxial or triaxial data be employed in its evaluation.

There are some immediately apparent circumstances that preclude the applicability of this failure theory. The first would be a concavity in the failure envelope. Such features are sometimes apparent with materials that exhibit buckling in biaxial compression (Rowlands, 1985). The modal theory presented in this thesis also produces convex envelope for all symmetries including isotropy (von Mises criteria). In fact, all of the anisotropic failure criteria suggested so far produce convex envelopes and would obviously not accommodate such a feature. Clearly, specially tailored empirical functions would have to be developed to describe the strength behavior of these materials.

Another circumstance that precludes the applicability of this theory is that of a material with a failure envelope that exhibits principal directions different from those of its elasticity tensor. The Kelvin mode failure surfaces are normal to the eigenstresses; therefore, implicit in the formulation is the prediction that both the strength and elasticity envelope share the same directions, though not necessarily the same aspect ratios or position in a principal stress space. Fortunately this assumption is one that is generally accepted for organic materials such as the wood and the bone data presented in this study.

This close connection between the elasticity and the Kelvin mode strength predictions requires not only that the material be linearly elastic within the failure bound but that the

anisotropy remain constant within it as well. This is not always the case, particularly for aggregates such as the concrete example illustrated in this study.

This modal failure theory represents one of the first attempts to correlate the failure stress of an anisotropic material with a failure mechanism. Some of the results presented in this study are encouraging but not conclusive. The paperboard biaxial modal failure envelope is in excellent agreement with experiment and appears to account for the discontinuities in the strength distribution reported by Suhling *et al.* (1985). However, no association of a failure mechanism with these strength data was reported. So it is impossible to tell if the failure data associated with a particular Kelvin or complementary mode can be can also be attributed to a particular failure mechanism.

It is a common premise of scientific investigations that experimentally measured data is the observed truth and that the theory which is meant to explain this data is an educated guess. A close match of the theoretical prediction with experiment is seen as a validation of the theory. But when the data does not fit, the explanation as to why this occurred is as significant as a validation itself. This was certainly the case for the concrete example. The data used to validate the modal failure envelope appears to have been beyond the applicable limits of the modal theory. Empirical curves, on the other hand, are not theories. They are meant to accommodate the experimental data as closely as possible regardless of how the data was obtained or what measure it is meant to represent. For instance, it is possible to fit an empirical correlation to the triaxial concrete strength data. Figure 16 illustrates two such curves. But these correlations are performed without regard to possible changes in the mechanical properties. Most of the anisotropic failure criteria to date are also empirical

curves. The Hill and Tsai-Wu type criteria are intended to fit the measured strengths with a smooth convex envelope. The belief that these criteria impose is that, if two similar stress states represent two failure points, then some in-between stress state must also be a similar failure point. When the Tsai-Wu is combined with a predictor of its coefficients, the resulting criterion is more than an empirical relation. The bovine Tsai-Wu eq.(9) of Cowin (1989) is such an example because the stress interactions terms $F_{i,j}$ are functions of the uniaxial and shear strengths (Cowin, 1979). The biaxial strength distribution is thus predicted from uniaxial and shear strengths. The modal energy failure criterion of Biegler and Mehrabadi (1993) is a genuine theory. This theory postulates that an anisotropic material fails when the energy in any one of its six independent modes has reached some critical value. The theory is entirely analogous to the theory of failure by maximum distortional or dilatation energy for isotropic materials. The superposition of the complementary modes is analogous to that of a maximum principal stress criterion over the distortional and dilatational energy criterion. The necessity of this additional set of failure modes became apparent after the observation that the modal energy criterion alone could not account for the different compressive and tensile strengths of paperboard. The Kelvin mode failure theory thus represents a genuine theory because it results in an explicit predictor of strength whereas the currently available correlation criteria such as those of Tsai-Wu and Hill can only offer an implicit prediction.

The implied correlation of the principal directions of the strength envelope with those of the elasticity tensor makes this theory unique. Organic materials such as wood and bone have demonstrated connection between their elasticity and strength, so that a failure theory such as this one may be particularly well suited for them.

The most significant remaining shortcoming of this modal failure theory is the likely requirement of an undetermined number of multiaxial tests to completely define the failure envelope. Indeed, because the Kelvin and complementary modes are not orthogonal to each other, it is likely that more than the twelve minimum mechanical tests would be required. An appropriate sequence of tests might be a set of three (positive and negative) pairs of uniaxial tests in the three principal directions of the material followed by three pairs of triaxial tests in the direction of the modal stresses. The three modal and three principal stress magnitudes would then be tabulated and the maximum and minimum values identified for each column. If only one mode (Kelvin or complementary) has reached an extremum at a particular strength data point, then that mode is presumed to have been uniquely determined and may safely be ignored in any subsequent iteration. If on the other hand, a strength data can be attributed to the extremum of two or more modes, then this point represents an ambiguity which must be resolved by additional mechanical tests. Fortunately, because all successive failure envelopes are necessarily convex, they also represent progressively less conservative failure predictions.

7 CONCLUSIONS AND RECOMMENDATIONS

The failure criterion of Biegler and Mehrabadi (1993) was introduced and the shortcomings of their procedure for the determination of the modal failure envelope was exposed. A refined procedure which involves the determination of the maximum and minimum modal stress magnitudes (Kelvin modes) rather than the modal energies was proposed. It was further shown that the Kelvin mode theory provides an incomplete description of the failure of some materials, but that this weakness can be addressed by the introduction of set of complementary modes. This combined modal theory was applied to seven numerical examples: an isotropic concrete, the tetragonal paperboard example used by Biegler and Mehrabadi (1993), two orthotropic softwoods, two orthotropic hardwoods, and an orthotropic cortical bone example. The resulting failure envelopes for these examples were plotted and, with the exception of concrete, shown to produce intuitively correct failure predictions. For concrete, the method appears to be inapplicable for the kind of failure data that is available, so its results are inconclusive. For paperboard, the inclusion of the biaxial strength data has improved the predictions of the modal failure theory. The Kelvin and complementary principal stress modes appear to better account for the paperboard strength distribution. For the four orthotropic woods, the theory produces intuitively correct predictions of multiaxial strength. For bovine cortical bone the results are inconclusive. A comparison of the triaxial prediction with an available Tsai-Wu was not possible because only the modal theory produced a bound in triaxial compression. The biaxial predictions of both theories, however, did not agree. Further comparison of these two competing predictions must be postponed until biaxial data for this material is available.

The value of this work lies in the nature of its strength predictions. The Kelvin mode criterion is based on the premise that an anisotropic elastic material will fail when the energy in any one of up to six independent modes has reached a critical value (Biegler and Mehrabadi, 1993). Because it is based on this premise the Kelvin mode criterion is an explicit predictor of the strength rather than implicit one such as the Tsai-Wu, Hill and other criteria. The Kelvin mode criterion is therefore a genuine theory of the multiaxial strength of any anisotropic elastic material and appears to be a viable and practical alternative to the Tsai-Wu and other current anisotropic strength criteria.

7.1 Recommendations and Future Outlook

The obvious lack of multidimensional failure data is a handicap for any multidimensional failure theory. This theory would greatly benefit from multiaxial mechanical test of any anisotropic material. An intriguing possibility is one which is presented by those materials for which the anisotropy is due to some obvious arrangement of the microstructure. For instance, the geometric arrangement of the trabeculae of cancellous bone may be used to reconstruct its microstructure as a finite element model. A simulated mechanical test may then be performed on the model of the sample. An appropriate plastic isotropic failure criterion may be assumed for the material of the trabeculae. The failure of cancellous bone structure may then be associated with the onset of a significant non-linear response of the entire cancellous bone model. The application of combined stress is a simple matter for a computer model so that any number of multiaxial tests can be performed on identical samples and without the nefarious effects of undesired boundary conditions. Such

an approach may be the only practical one for small highly porous materials.

Although, theoretically, triaxial testing would be ideal for the determination of the modal failure envelope, current methods may be inadequate to provide accurate measurements. A more practical approach would be to perform a series of biaxial tests in the three orthogonal planes of symmetry. This may prove to be sufficient if, for a given material, each mode (Kelvin or complementary) can be associated with a unique set of strength data.

8 APPENDIX

Table 7 Estimate of the biaxial failure data reported by Suhling *et al* (1985). All units are in MPa

T_2 -T_3 Biaxial Failure data				T_1 -T_3 Biaxial Failure data			
T_1, T_2, T_3	Kelvin mode			$T_2T_2T_3$	Kelvin mode		
	1	2	3		1	2	3
0.0,0.0,56.0	47.10	30.28	0	0.0,0.0,56.0	47.10	30.28	0
0.0,7.0,55.0	48.93	25.58	-4.94	7.0,0.0,55.0	48.93	25.58	4.94
0.0,7.0,53.0	47.25	24.50	-4.94	7.0,0.0,53.0	47.25	24.50	4.94
0.0,26.0,56.0	57.04	14.82	-18.38	26.0,0.0,56.0	57.04	14.82	18.38
0.0,26.0,54.0	55.36	13.74	-18.38	26.0,0.0,54.0	55.36	13.74	18.38
0.0,24.0,54.0	54.59	14.93	-16.97	24.0,0.0,54.0	54.59	14.93	16.97
0.0,36.0,44.0	50.77	2.38	-25.45	36.0,0.0,44.0	50.77	2.38	25.45
0.0,37.0,36.0	44.43	-2.53	-26.16	37.0,0.0,36.0	44.43	-2.53	26.16
0.0,36.0,35.0	43.20	-2.48	-25.45	36.0,0.0,35.0	43.20	-2.48	25.45
0.0,35.0,34.0	41.98	-2.42	-24.74	35.0,0.0,34.0	41.98	-2.42	24.74
0.0,32.0,10.0	20.64	-13.62	-22.62	32.0,0.0,10.0	20.64	-13.62	22.62
0.0,36.0,13.0	24.70	-14.38	-25.45	36.0,0.0,13.0	24.70	-14.38	25.45
0.0,37.0,14.0	25.92	-14.43	-26.16	37.0,0.0,14.0	25.92	-14.43	26.16
0.0,30.0,0.0	11.47	-17.84	-21.21	30.0,0.0,0.0	11.47	-17.84	21.21
0.0,26.0,-11.0	.69	-21.41	-18.38	26.0,0.0,-11.0	.69	-21.41	18.38
0.0,24.0,-15.0	-3.43	-22.38	-16.97	24.0,0.0,-15.0	-3.43	-22.38	16.97
0.0,21.0,-17.0	-6.26	-21.68	-14.84	21.0,0.0,-17.0	-6.26	-21.68	14.84
0.0,22.0,-15.0	-4.20	-21.19	-15.55	22.0,0.0,-15.0	-4.20	-21.19	15.55
0.0,16.0,-18.0	-9.02	-19.25	-11.31	16.0,0.0,-18.0	-9.02	-19.25	11.31
0.0,12.0,-19.0	-11.39	-17.41	-8.48	12.0,0.0,-19.0	-11.39	-17.41	8.48
0.0,11.0,-21.0	-13.45	-17.90	-7.77	11.0,0.0,-21.0	-13.45	-17.90	7.77
0.0,11.0,-20.0	-12.61	-17.35	-7.77	11.0,0.0,-20.0	-12.61	-17.35	7.77
0.0,5.0,-19.0	-14.06	-13.24	-3.53	5.0,0.0,-19.0	-14.06	-13.24	3.53
0.0,0.0,-20.0	-16.82	-10.81	0	0.0,0.0,-20.0	-16.82	-10.81	0
0.0,-3.0,-18.0	-16.28	-7.95	2.12	-3.0,0.0,-18.0	-16.28	-7.95	-2.12
0.0,-5.0,-17.0	-16.21	-6.22	3.53	-5.0,0.0,-17.0	-16.21	-6.22	-3.53

Continued on next page

Table 7 -Continued

T_2 -T_3 Biaxial Failure data				T_1 -T_3 Biaxial Failure data			
T_1,T_2,T_3	Kelvin mode			$T_2T_2T_3$	Kelvin mode		
	1	2	3		1	2	3
0.0,-7.0,-18.0	-17.81	-5.57	4.94	-7.0,0.0,-18.0	-17.81	-5.57	-4.94
0.0,-8.0,-17.0	-17.35	-4.43	5.65	-8.0,0.0,-17.0	-17.35	-4.43	-5.65
0.0,-9.0,-16.0	-16.89	-3.30	6.36	-9.0,0.0,-16.0	-16.89	-3.30	-6.36
0.0,-11.0,-12.0	-14.30	.05	7.77	-11.0,0.0,-12.0	-14.30	.05	-7.77
0.0,-13.0,-12.0	-15.06	1.24	9.19	-13.0,0.0,-12.0	-15.06	1.24	-9.19
0.0,-13.0,-8.0	-11.70	3.40	9.19	-13.0,0.0,-8.0	-11.70	3.40	-9.19
0.0,-13.0,-7.0	-10.85	3.94	9.19	-13.0,0.0,-7.0	-10.85	3.94	-9.19
0.0,-12.0,-6.0	-9.63	3.89	8.48	-12.0,0.0,-6.0	-9.63	3.89	-8.48
0.0,-13.0,-6.0	-10.01	4.48	9.19	-13.0,0.0,-6.0	-10.01	4.48	-9.19
0.0,-12.0,-2.0	-6.27	6.05	8.48	-12.0,0.0,-2.0	-6.27	6.05	-8.48
0.0,-11.0,0.0	-4.20	6.54	7.77	-11.0,0.0,0.0	-4.20	6.54	-7.77
0.0,-13.0,0.0	-4.97	7.73	9.19	-13.0,0.0,0.0	-4.97	7.73	-9.19
0.0,-12.0,7.0	1.29	10.92	8.48	-12.0,0.0,7.0	1.29	10.92	-8.48
0.0,-14.0,12.0	4.73	14.81	9.89	-14.0,0.0,12.0	4.73	14.81	-9.89
0.0,-13.0,17.0	9.32	16.92	9.19	-13.0,0.0,17.0	9.32	16.92	-9.19
0.0,-11.0,11.0	5.04	12.49	7.77	-11.0,0.0,11.0	5.04	12.49	-7.77
0.0,-11.0,13.0	6.72	13.57	7.77	-11.0,0.0,13.0	6.72	13.57	-7.77
0.0,-12.0,12.0	5.50	13.62	8.48	-12.0,0.0,12.0	5.50	13.62	-8.48

The extreme values for each mode are selected. We therefore get a set of six criteria for three Kelvin and three complementary modes

Kelvin modes:

$\sigma^{(1)}_{max} = 57.0$ and $\sigma^{(1)}_{min} = -17.8$

$\sigma^{(2)}_{max} = 30.3$ and $\sigma^{(2)}_{min} = -22.4$

$\sigma^{(3)}_{max} = 26.2$ and $\sigma^{(3)}_{min} = -26.2$

Complementary modes:

$\sigma_P{}^{(1)}_{max} = (T_1)_{max} = 37.0$ and $\sigma_P{}^{(1)}_{min} = (T_1)_{min} = -14$

$\sigma_P{}^{(2)}_{max} = (T_2)_{max} = 37.2$ and $\sigma_P{}^{(2)}_{min} = (T_1)_{min} = -14$

$\sigma_P{}^{(3)}_{max} = (T_3)_{max} = 56.0$ and $\sigma_P{}^{(3)}_{min} = (T_3)_{min} = -21$

(All units are in MPa.)

9 BIBLIOGRAPHY

Biegler, M. W., and Mehrabadi, M. M., 1995, "An energy-based constitutive model for anisotropic solids subject to damage", Mechanics of Materials, Vol. 19, pp. 151-164

Biegler, M. W., and Mehrabadi, M. M., 1993, "An energy-based failure criterion for anisotropic solids subject to damage", *Studies in Applied Mechanics*, Vol. 34, pp. 23-34.

Bridgeman, P.,(1923) "The compressibility of thirty metals", Proc. Am. Acad. Arts Sci., Vol. 58:5, p. 164-242.

Cowin, S.C. (1979) "On the Strength and Anisotropy of Bone and Wood". *J. Applied Mechanics*, Vol. 46:4, 832-838.

Cowin, S.C. (1989) *Bone Mechanics*. CRC Press, Boca Raton.

Cowin, S.C. and Mehrabadi, M.M., (1995a) "Identification of the Elastic Symmetry of Bone and Other Materials". *J. Biomechanics.*, Vol. 22:6/71, pp. 503-515.

Cowin, S.C. and Mehrabadi, M.M., (1995b) "Anisotropic Symmetries of Linear Elasticity". *J. Applied Mechanics*, Vol. 48, pp. 247-285.

Cowin, S.C. and Yang, G., (1997) "Averaging Anisotropic Elasticity Constant Data". *J. Elasticity*, Vol. 18, pp. 151-180.

Feng, W. W., (1991), "A Failure Criterion for Composite Materials", *Journal of Composite Materials*, Vol. 25, p.88.

Forest Products Laboratory. (1974). *Wood Handbook: Wood as an Engineering Material.* Agriculture Handbook No.72. U.S. Dept. Of Agriculture, Washington D.C..

François, M., (1995). *Identification des Symétries Matérielles de Matériaux Anisotrope.* Ph.D. Thesis, l'Université Pierre et Marie Curie (Paris 6) FRANCE.

Hashin, Z., 1980, "Failure Criteria for Unidirectional Fiber Composites", J. Appl. Mech., Vol. 47, p.329.

Harrigan, T. P., Jasty, M., Mann, R. W., and Harris, W. H.,(1988), "Limitations of the Continuum Assumption in Cancellous Bone", *J. Biomechanics*, Vol. 21:4, pp. 269-275.

Hill, R., (1950), *The Mathematical Theory of Plasticity*, Oxford University Press, London.

Hobbs, D. W., and Pomeroy, C. D. (1974), *The Structural Engineer*, Oxford University Press, London. Quoted in Wang C.Z., Guo, Z. H., Zhang, X. Q., (1987) "Experimental Investigation of Biaxial and Triaxial Compressive Concrete Strength". *ACI. Materials Journal*, Vol. 84-M11 , pp. 92-100.

Kupfer H. B. and Gerstle, K. H. 1973, "Behavior of Concrete Under Biaxial Stresses", *J. Engr. Mech. Division*, Proc. ASCE, Vol. 99 No. EM4, pp. 853-866.

Lade, P. V., and Duncan, (1973) J. M., "Cubical Triaxial Tests on Cohesionless Soil", *Journal of the Soil Mechanics and Foundations Division,* ASCE, Vol. 99, No. SM10, Oct., pp. 793-812.

Liu J. Y., (1984) "Evaluation of the Tensor Polynomial Strength Theory for Wood", *Journal of Composite Materials,* Vol 18, pp. 216-225.

Lord Kelvin, (1856), Elements of a Mathematical Theory of Elasticity, Phil. Trans. R. Soc. Vol. 166, p. 481.Quoted in Mehrabadi, M.M. and Cowin, S.C., (1990) "Eigentensors of Linear Anisotropic Elastic Materials". *J. Mech. Appl. Math.*, Vol. 43, pp.15-41.

Martin D. W., (1994), "An Energy Based Model for Predicting the Elastic-Plastic Response and Failure of Anisotropic Materials",Master's Thesis, Tulane University.

Mehrabadi, M.M. and Cowin, S.C., (1990) "Eigentensors of Linear Anisotropic Elastic

Materials". *J. Mech. Appl. Math.*, Vol. 43, pp.15-41.

Nadai, A. *Theory of flow and fracture of materials*, McGraw-Hill, 1950

Newman, K. And Newman J. B., (1971) "Failure Theories and Design Criteria for Plain Concrete". *Proceedings*, Structure, Solid Mechanics, and Engineering Design, Wiley-Interscience, London, pp. 15-41. Quoted in Wang C.Z., Guo, Z. H., Zhang, X. Q., (1987) "Experimental Investigation of Biaxial and Triaxial Compressive Concrete Strength". *ACI. Materials Journal*, Vol. 84-M11 , pp. 92-100.

Rowlands, R. E., (1985), "Strength (Failure) Theories and their Experimental Correlation", *Handbook of Composites, Vol. 3 - Failure Mechanics of Composites,* (eds. G. C. Sih and A. M. Skudra), Elsevier Science Publishers B. V., pp 71-125

Rychlewski, J., (1984), "On Hook's Law", *Prikl. Matem. Mekhan.*,Vol. 48:3, pp. 303-314.

Suhling, J. C., Rowlands, R. E., Johnson, M. W. and Gunderson, D. E., 1985, "Tensorial Strength Analysis of paperboard", *Experimental Mechanics*. Vol. 25. P.75-84

Schreyer, H. L., and Zuo, Q. H., 1995, "Anisotropic Yield Surfaces Based on Elastic Projection Operators", *J Appl. Mech.*, Vol. 62, pp.780-785.

Schniewind A.P. (1979)"Mechanical behavior and Properties of Wood", *Wood: Its Structure and Properties*". Wangaard F.F. ed., EMMSE, Pennsylvania State University, Vol. 1.pp 233-270

Tsai, S. W., and Wu, E. M., 1970, "A General Theory of Strength for Anisotropic Materials", *Journal of Composite Materials*, Vol. 5, pp.58-80.

Tryding, J., 1994, "A Modification of the Tsai-Wu failure criterion for biaxial strength of paper", *Tappi Journal* , Vol. 77:8 pp.132-134.

Wang C.Z., Guo, Z. H., Zhang, X. Q., (1987) "Experimental Investigation of Biaxial and Triaxial Compressive Concrete Strength". *ACI. Materials Journal*, Vol. 84-M11 , pp. 92-100.

Wu E. M. and Scheublein J. K., (1974) "Lamina Strength - A Direct Characterization Procedure". *Composite Materials: Testing and Design (3rd conference)*, ASTM STP 546 , American Society for Testing and Materials, pp. 188-206.